livers

MDPI

Article

Targeted Liver Fibrosis Therapy: Evaluating Retinol-Modified Nanoparticles and Atorvastatin/JQ1-Loaded Nanoparticles for Deactivation of Activated Hepatic Stellate Cells

Aya A. Ezzat [1,*], Salma N. Tammam [1], Ralf Weiskirchen [2], Sarah K. Schröder-Lange [2] and Samar Mansour [1,3,*]

[1] Department of Pharmaceutical Technology, Faculty of Pharmacy and Biotechnology, German University in Cairo (GUC), Cairo 11835, Egypt; salma.tammam@gmail.com
[2] Institute of Molecular Pathobiochemistry, Experimental Gene Therapy and Clinical Chemistry (IFMPEGKC), RWTH University Hospital, D-52074 Aachen, Germany; rweiskirchen@ukaachen.de (R.W.); saschroeder@ukaachen.de (S.K.S.-L.)
[3] Faculty of Pharmaceutical Engineering and Technology, German International University (GIU), Cairo 11351, Egypt
* Correspondence: aya.ezzat-ali@guc.edu.eg or aya.as.ezzat@gmail.com (A.A.E.); samar.mansour@guc.edu.eg or samar_holayel@yahoo.com (S.M.); Tel.: +20-1000587685 (A.A.E.); +20-1023433669 (S.M.)

Abstract

Background: Liver fibrosis is a progressive pathological condition characterized by excessive extracellular matrix deposition, driven by activated hepatic stellate cells (aHSCs). Effective therapeutic strategies require targeting aHSCs and agents capable of reversing their activated phenotype. **Methods**: In this study, we developed chitosan nanoparticles loaded with atorvastatin (AS) and JQ1 and functionalized them with varying densities of retinol (Rt) to exploit aHSC targeting. **Results**: In vitro, Rt-NPs demonstrated enhanced uptake in GRX cells, with optimal performance observed at high Rt density (HRt-NPs). In vivo biodistribution in CCl_4-induced fibrotic and healthy mice revealed that LRt-NPs achieved superior hepatic accumulation in fibrotic livers compared to unmodified and HRt-NPs, underscoring the importance of optimal ligand density for targeting. Western blot analysis showed that treatment of GRX cells with Rt-AS-NPs and Rt-JQ1-NPs either individually or combined significantly reduced the expression of fibronectin, vimentin, and PDGFR-β, key markers of HSC activation, with combination therapy providing more significant effects. **Conclusions**: This work highlights the potential of Rt-chitosan NPs loaded with AS and JQ1 as an effective dual-drug system for targeted antifibrotic therapy, offering enhanced hepatic selectivity, improved safety, and potent aHSC deactivation.

Keywords: liver fibrosis; chitosan nanoparticles; targeting; retinol; hepatic stellate cells; atorvastatin; JQ1; anti-fibrotic therapy

check for updates

Academic Editor: Byoung Kuk Jang

Received: 21 August 2025
Revised: 27 September 2025
Accepted: 12 November 2025
Published: 5 December 2025

Citation: Ezzat, A.A.; Tammam, S.N.; Weiskirchen, R.; Schröder-Lange, S.K.; Mansour, S. Targeted Liver Fibrosis Therapy: Evaluating Retinol-Modified Nanoparticles and Atorvastatin/JQ1-Loaded Nanoparticles for Deactivation of Activated Hepatic Stellate Cells. *Livers* **2025**, *5*, 63. https://doi.org/10.3390/livers5040063

Copyright: © 2025 by the authors. Licensee MDPI, Basel, Switzerland. This article is an open access article distributed under the terms and conditions of the Creative Commons Attribution (CC BY) license (https://creativecommons.org/licenses/by/4.0/).

1. Introduction

Fibrotic diseases, marked by excessive extracellular matrix (ECM) deposition resulting from dysregulated wound healing and connective tissue repair, pose a major global health burden, accounting for nearly 45% of mortality in developed countries [1]. In the liver, fibrosis is driven by the activation of hepatic stellate cells (HSCs), which typically make up 5–10% of the liver cell population and are located in the space of Disse [2]. Quiescent HSCs store vitamin A, but in response to liver injury, they transdifferentiate into myofibroblast-like cells (HSC-MFBs) under the influence of fibrogenic mediators like TGF-β1 and PDGF.

This activation leads to increased expression of α-smooth muscle actin (α-SMA), ECM synthesis, and secretion of collagen I/III, resulting in changes to the quantity and quality of the ECM [3].

As fibrosis progresses, ECM proteins such as fibronectin, collagen, and laminin can increase up to tenfold, disrupting the normal hepatic architecture. Sinusoidal capillarization, characterized by the loss of fenestrations and the replacement of the discontinuous sinusoidal endothelium with a basement membrane, further exacerbates liver dysfunction. Impaired ECM degradation caused by elevated levels of tissue inhibitors of metalloproteinases (TIMPs), contributes to the formation of scars, cirrhosis, and increased risk of hepatocellular carcinoma (HCC) risk [4,5].

Despite this, fibrosis may be reversible [6]. Statins, in addition to their lipid-lowering activity, exhibit anti-fibrotic, anti-inflammatory, antioxidant, and anti-proliferative properties. They inhibit HSC activation and collagen deposition, as demonstrated in bile duct ligation (BDL) models treated with atorvastatin. Clinically, statin therapy is linked to slower fibrosis progression in HCV patients [7], improved perfusion in cirrhosis [8], reduced ROS, enhanced nitric oxide production [9], and free radical scavenging [10].

Bromodomain-containing protein 4 (BRD4) is another promising antifibrotic target. As an epigenetic regulator, BRD4 binds acetylated lysines, promoting pro-fibrotic gene expression and myofibroblast differentiation [11–13]. BET inhibitors such as JQ1 block BRD4 binding to acetylated histones, reducing fibrosis-related gene expression. JQ1 suppresses HSC activation, downregulates α-SMA, and interferes with JAK2/STAT3 signaling, showing efficacy in multiple organ fibrosis models [14–16].

Due to the multifactorial nature of fibrosis, single-agent therapy may not be sufficient. Combination therapy is appealing, as atorvastatin and JQ1 act through distinct but complementary pathways to modulate HSCs. However, both drugs have poor water-solubility, and JQ1 may have potential off-target effects. Nanoparticle (NP)-based delivery can address these challenges by enhancing solubility, stability, pharmacokinetics, and safety, while enabling targeted delivery.

The retinol-binding protein (RBP) receptor, crucial for vitamin A uptake in quiescent HSCs, is upregulated in activated HSCs and provides a selective target for NP-based therapy [17–23].

Our previous work demonstrated that retinol-modified NPs efficiently target HSCs and that atorvastatin–JQ1 combinations synergistically prevent HSC activation. Here, we extend these findings to test whether this dual-drug strategy can deactivate activated HSCs (aHSCs), reverse established fibrosis, and determine if retinol modification enhances targeted delivery to fibrotic liver tissue.

2. Materials and Methods

2.1. NP Formulation and Characterization

Chitosan NPs were formulated through ionotropic gelation between chitosan and sodium tripolyphosphate (TPP). In brief, a 0.5% (*w*/*w*) solution of low molecular weight chitosan (Sigma-Aldrich, Darmstadt, Germany) at pH 4 was mixed with an equal volume of 0.125% (*w*/*w*) TPP (Mistral Chemicals, Moira, Northern Ireland, UK) by stirring for 30 min at 1000 rpm. The average hydrodynamic diameter (HD) and zeta potential (ZP) of the NPs were measured using a Malvern Zetasizer Nano ZS90 (Malvern Instruments Ltd., Malvern, Worcestershire, UK) with a 90° scattering angle at 25 °C. Three independently prepared batches of NPs were analyzed in deionized water, and the results were expressed as mean ± standard deviation (SD). For the study of NP morphology, a drop of NP suspension was deposited onto an aluminum foil-coated glass slide. The slide was allowed to dry, and then a thin layer of gold was sputtered onto the sample using a Polaron SC7640

Sputter Coater (Quorum Technologies Ltd., Newhaven, UK) under an argon atmosphere. The sputtering process lasted for 2 min at a current of 20 mA. Subsequently, the samples were analyzed using a field emission scanning electron microscope (Hitachi S-2460N SEM, Hitachi Ltd., Tokyo, Japan) [24].

2.2. NP Modification with Different Densities of Retinol

To introduce retinol (Rt) (Sigma Aldrich, Darmstadt, Germany) onto the NPs, 1,1-carbonyldiimidazole (CDI) (Sigma Aldrich, Darmstadt, Germany) was employed as a hydroxyl amine crosslinker to connect the hydroxyl (OH) groups of retinols with the amino (NH_2) groups of chitosan. A stock solution of Rt-CDI was prepared at a concentration of 3.33 mg/mL in terms of Rt, by combining a solution of 5 mg/mL retinol in DMSO with a solution of 12 mg/mL CDI in DMSO. The reaction took place overnight in a shaking incubator, maintained at a speed of 100 rpm in the dark at a temperature of 37 °C. The NPs were initially prepared and then purified by centrifugation at 14,000 rpm (20,817 rcf) for 30 min at 25 °C. The NP pellets were reconstituted to the initial volume in deionized water, subsequently, increasing concentrations (30–150 µg/mL) of the Rt-CDI solution were incubated with 500 µL aliquots of the NPs. The incubation was carried out overnight in a shaking incubator at 100 rpm, in the dark, and at a temperature of 37 °C. This process resulted in the generation of NPs with varying densities of Rt, corresponding to the different concentrations of Rt-CDI employed. The Rt-NPs were subjected to centrifugation at 14,000 rpm (20,817 rcf) for 30 min at a temperature of 25 °C. The resulting pellets were then dissolved in DMSO, allowing for the quantification of the attached Rt molecules. The quantification was performed using fluorometry, with excitation at a wavelength of 335 nm and emission at 458 nm. To determine the number of Rt molecules per NP (Rt/NP), as well as the number of Rt molecules per square nanometer (Rt/nm^2), Equations (1)–(5) and (1)–(7) were utilized, respectively [25].

$$\text{Volume of polymer used in NPs formulation} = \text{mass of polymer used in NPs formulation/density of polymer} \quad (1)$$

$$\text{Volume of NP} = 4/3\ \pi\ \text{r3 where r is the NP radius} \quad (2)$$

$$\text{Number of NPs} = \text{volume of polymer used in NPs formulation/volume of one NP} \quad (3)$$

$$\text{Number of tagged Rt molecules} = \text{amount of tagged Rt/molecular weight of Rt} * \text{Avogadro's number} \quad (4)$$

$$\text{Number of Rt on one NP} = \text{number of Rt/number of NPs} \quad (5)$$

$$\text{Area of NP} = 4\ \pi\ r^2 \quad (6)$$

$$\text{Number of Rt/nm}^2 = \text{number of Rt on one NP/area of one NP} \quad (7)$$

The experiment was conducted in triplicate, and the results were expressed as mean ± SD. Based on the results obtained, two concentrations of Rt were selected to represent low retinol (LRt) and high retinol (HRt) densities. The particle size and zeta potential of both formulations were determined according the method outlined in Section 2.1.

2.3. Drug Loading and Encapsulation Efficiency (EE%) Determination

2.3.1. Preparation of Atorvastatin NPs (AS-NPs)

The AS-NPs were prepared by following the procedure outlined above. However, prior to adding to the chitosan solution, either 3.5, 15, or 20 µL of a 37.5 mg/mL AS (EPICO Pharmaceuticals, Cairo, Egypt) in methanol solution per mL of TPP were added.

2.3.2. Preparation of (+)-JQ-1-NPs

The JQ1-NPs were prepared using the same methodology as described above. However, different volumes of 8 mg/mL JQ1 (MedChemExpress, Monmouth Junction, NJ, USA) in DMSO solution (17, 20, 25, 35, or 40 µL) were added per mL of TPP before combining with the chitosan solution. To determine the concentration of encapsulated drugs within the NPs, the NPs were centrifuged at 14,000 rpm (20,817 rcf) for 30 min. The concentration of the unencapsulated AS in the resulting supernatants was measured using our in-house UPLC-MS/MS method, previously developed by our group [25]. Similarly, the concentration of the unencapsulated JQ1 was measured using spectrophotometry at a wavelength of 300 nm. To calculate the encapsulated concentration of both drugs, the concentration of unencapsulated drug in the supernatant was subtracted from the total concentration of drug initially added. The encapsulation efficiency (EE%) and loading capacity (LC) were determined using the following equations from three independent batches of preparations, and the results were expressed as the mean ± SD.

$$LC = ((total\ amount\ of\ drug - free\ drug))/(nanoparticles\ weight)$$

$$EE\ \% = ((total\ amount\ of\ drug - free\ drug))/(total\ amount\ of\ drug) * 100$$

2.4. Evaluation of NPs Uptake in GRX Cells

Fluorescently labeled NPs (Fl-NPs) were prepared by dissolving fluorescein (Sigma Aldrich, Darmstadt, Germany) in DMSO to achieve a final concentration of 40 mg/mL. Then, 16 µL of the fluorescein stock solution was added per mL of TPP solution before mixing with the chitosan solution to prepare the NPs as described above. To isolate the Fl-loaded NPs and remove any excess unencapsulated fluorescein, the NP suspension underwent centrifugation at 14,000 rpm (20,817 rcf) for 30 min at a temperature of 25 °C. After centrifugation, the NPs were reconstituted using ultrapure H_2O and modified with retinol to obtain low-retinol Fl-NPs (LRt-Fl-NPs) and high-retinol Fl-NPs (HRt-Fl-NPs). The GRX cells (Banco de Células do Rio de Janeiro, Rio de Janeiro, Brazil (BCRJ code: 0094) were seeded in 96-well plates at a density of 10^4 cells per well. After 24 h, the cells were treated with either 100 µL of cell culture media containing 7 mM retinol or fresh cell culture media for 1 h. Then, all media were removed, and Fl-NPs, LRt-Fl-NPs, and HRt-Fl-NPs were added to the cells at concentrations of 2 mg/mL. The cells were then incubated with the NPs for 24 h. The next day, the media containing the NPs were aspirated, the cells were washed twice with PBS, and the extent of NP uptake was determined using fluorometry with an excitation wavelength of 494 nm and an emission wavelength of 512 nm. Calibration curves specific to each type of NPs (Fl-NPs, LRt-Fl-NPs, and HRt-Fl-NPs) were used for quantification. The results were expressed as the mean ± SD for a sample size of 5 (n = 5).

Furthermore, since GRX cells represent aHSCs and consequently produce excess extracellular matrix, we wanted to test the impact of pretreatment with collagenase on NPs uptake. GRX cells were seeded in 96-well plates at a density of 10^4 cells per well. After 24 h, the cells were treated with 100 µL of collagenase-loaded NPs (Col-NPs) suspended in cell culture media equivalent to (0.5 mg/mL) of collagenase, or left untreated (fresh cell culture media). These treatments were performed for a duration of 12 h at 37 °C. Following the treatment period, all media were aspirated, and Fl-NPs, LRt-Fl-NPs, or HRt-Fl-NPs were added to the cells at a concentration of 2 mg/mL. The NPs were incubated with the cells for 24 h. Subsequently, the NP-containing medium was aspirated, the cells were washed twice with PBS, and the extent of NP uptake was measured using fluorometry with an excitation wavelength of 494 nm and an emission wavelength of 512 nm. Calibration curves specific to each type of NPs (Fl-NPs, LRt-Fl-NPs, and HRt-Fl-NPs) were employed for accurate quantification. The results were expressed as the mean ± SD for a

sample size of 5 (n = 5). Collagenase-loaded NPs (Col-NPs) were prepared by dissolving 12 mg of collagenase (Collagenase H (0.23 U/mg) from *Clostridium histolyticum* (Roche, Basel, Switzerland)) in each 1 mL of the TPP solution before it was added to an equal volume of the chitosan solution, and then the NPs preparation proceeded as mentioned above. To quantify the encapsulated amount, Col-NPs were separated from un-entrapped collagenase by centrifugation at 14,000 rpm (20,817 rcf) for 30 min at 25 °C. A protein content assay was conducted spectrophotometrically (Double Beam Spectrophotometer: V-530 UV/Visible Spectrophotometer Jasco, Hachioji, Tokyo, Japan) on the supernatant using the Coomassie Plus (Bradford) Assay Kit (Pierce Biotechnology, Rockford, IL, USA) as described in previous work from our group [26].

2.5. Effect of Retinol Tagging on NP Bio-Distribution

2.5.1. Induction of Liver Fibrosis

A total of 106 male Swiss albino mice, aged 8 weeks and weighing 25–30 g, were obtained from the National Research Center in Cairo, Egypt. The experimental procedures and animal care followed the ethical guidelines of the Research Ethics Committee of the Faculty of Pharmacy and Biotechnology at the German University in Cairo (protocol code PTC-2020-09-SMH and date of approval 7 September 2020). Upon arrival, the mice were allowed to acclimate for a period of 7 days in cages maintained at room temperature with a 12 h light/dark cycle. They had ad libitum access to standard rodent food and tap water throughout the acclimatization period and the study. The mice were divided into two groups, each consisting of 53 animals. The first group received intra-peritoneal (IP) injections of a 10% *v/v* solution of carbon tetrachloride (CCl_4) (ADWIC, Cairo, Egypt) in olive oil at a volume of 2.5 µL per gram of body weight. These injections were administered twice a week for a duration of one month to induce chronic liver damage. The second group served as the control and received the same volume of olive oil through IP injections.

2.5.2. Histopathology Analysis

After one month, 5 mice from each group were sacrificed and their livers were harvested. The collected liver tissues were carefully washed with water to remove any external contaminants, and then a portion of each was fixed in 10% formal saline solution for 24 h. Following fixation, the tissues were rinsed with water once again. To prepare the tissues for histological examination, a series of alcohol dilutions including methyl, ethyl, and absolute ethyl alcohol were used to dehydrate the specimens. Subsequently, the tissues were cleared using xylene, which helped remove the alcohol and allowed the tissues to become transparent. The dehydrated and cleared liver tissues were embedded in paraffin blocks and placed in a hot air oven set at 56 °C for 24 h. This process facilitated the infiltration of the tissues with paraffin, ensuring their preservation and structural integrity. Once the paraffin blocks were prepared, thin sections with a thickness of 4 µm were obtained using a sledge microtome. The resulting tissue sections were carefully collected on glass slides. To prepare the sections for microscopic examination, the paraffin was removed from the slides through a deparaffinization process. Then, the sections were stained with a combination of hematoxylin and eosin (H&E), which provided contrast and enabled the visualization of cellular structures. Finally, the stained sections were observed under a light microscope (OLYMPUS BX63) for further analysis and evaluation.

2.5.3. Collagen Quantification

A portion of each mouse liver tissue was homogenized in PBS using an Ultra-Turrax homogenizer, yielding homogenates with a tissue concentration of 0.3 g/mL for quantifying the expression of type III collagen. Initially, total RNA extraction was accomplished utilizing commercially available Silica-Magnetic NPs following the manufacturer's in-

structions (REME-D, Cairo, Egypt). Subsequently, cDNA synthesis and polymerase chain reaction (PCR) were carried out concurrently using a one-step reverse transcription PCR (RT-PCR) kit (# AE411-02, Transgen biotech LTD, Beijing, China). The primer sequences and thermal cycling conditions utilized for the RT-PCR analysis are detailed in Table 1 and Table 2, respectively. Gel electrophoresis was then performed on the PCR products utilizing a 3% agarose gel and 1× Tris-Acetate buffer as the running buffer. Ethidium Bromide (10 mg/mL) was introduced for visualization under a UV transilluminator. The resulting bands were compared against the 50 bp ladder from GeneDireX (Taoyuan, Taiwan). Finally, the intensities of the bands were quantified using ImageJ software (Wayne Rasband, Kensington, MD, USA, version 1.53t) to assess and analyze the expression levels of the target gene.

Table 1. Primer sequence for collagen quantification.

Gene	Primer Sequence	Reference
Collagen 3α1	Forward: 5′-TGATGGGATCCAATGAGGGAGA-3′ Reverse: 5′-GAGTCTCATGGCCTTGCGTGTTT-3′	[27]

Table 2. Thermal cycling conditions for one step RT-PCR.

Step	Temperature	Time	No. of Cycles
Reverse transcription	45 °C	25 min	1
RT inactivation/initial denaturation	94 °C	4 min	1
Amplification	94 °C 57 °C 72 °C	30 s 30 s 1–2 kb/min	40
Final extension	72 °C	7 min	1

2.5.4. NP Administration

Following the in vitro uptake experiment and the observed impact of retinol modification on the efficiency of NPs uptake, we aimed to investigate the effect of retinol modification on the targeting ability of NPs in an in vivo setting. Accordingly, the remaining 48 animals in each group were further divided into 2 subgroups (**Schematic diagram in** Figure A1). The first subgroup received no treatment, while the other subgroup received three intravenous injections of Col-NPs over the course of one week, with injections administered on alternate days. The collagenase dose was 4.1 mg/kg/injection After this week of treatment, the subgroups were divided once again into four smaller subgroups, each containing 6 mice. The first subgroup served as the negative control, receiving no additional treatment. The second subgroup received three intravenous injections of Fl-NPs, the third subgroup received three intravenous injections of LRt-Fl-NPs, and the fourth subgroup received three intravenous injections of HRt-Fl-NPs. There was a two-hour interval between each pair of injections, and one hour after the final injection, all mice were sacrificed. Upon sacrifice, all organs, including the liver, kidneys, heart, and brain, were collected and washed with saline. The organs were then weighed, and subsequently, homogenized in PBS using an Ultra-Turrax homogenizer, resulting in a final tissue concentration of 0.3 g/mL. From each homogenate, 100 µL was added to 96-well plates, and the fluorescence intensity was measured using a plate reader set at an excitation wavelength of 494 nm and an emission wavelength of 512 nm. The fluorescence intensity of each well was normalized to the value of the negative control within the same treatment group to

determine the change in fluorescence intensity resulting from NP accumulation. All preparations used in the study were prepared under sterile conditions, and concentrated saline solutions were employed to adjust the formulations to an isotonic state. This adjustment aimed to minimize any potential irritation or discomfort experienced by the animals.

2.6. Effect of Drug-Loaded NPs on Cell Viability

GRX cells were seeded in 96-well plates at a density of 2.5×10^4 cells per well and allowed to adhere for 24 h. Subsequently, the culture media were removed, and the cells were treated with various formulations including free JQ1, JQ1-NPs, Rt-JQ1-NPs, free AS, AS-NPs, or Rt-AS-NPs at different concentrations for a duration of 24 h. After the treatment period, the media containing the free drugs or drug-loaded NPs were aspirated, the cells were washed with PBS, and the cell viability was assessed using the MTT assay. To account for any potential effects of chitosan and retinol on the cells, some cells were treated with NPs or Rt-NPs at concentrations equivalent to the highest concentrations of drug-loaded NPs used, based on polymer concentration. The experiment was conducted in quadruplicate, and the results were presented as the mean ± SD. The percentage of cell viability was determined using the following formula:

$$\%\ cell\ viability = (Absorbance\ of\ treated\ cells)/(Absorbance\ of\ control\ untreated\ cells) \times 100$$

2.7. Assessment of the Ability of Drug-Loaded NPs to Deactivate aHSCs

The evaluation of NPs' ability to deactivate activated hepatic stellate cells (aHSCs) was conducted using Western blot analysis. Fibronectin, Vimentin, and PDGFR-β expression served as the read-out system. GRX cells were seeded in 6-well plates at a density of 2×10^5 cells per well and treated one day after seeding. They were exposed to either 10 μM of free JQ1 or an equivalent amount of JQ1-NPs or Rt-JQ1-NPs, encapsulating 10 μM of JQ1. In addition, some cells were treated with 20 μM of free AS or an equivalent amount of AS-NPs or Rt-AS-NPs, encapsulating 20 μM of AS. Some cells were also simultaneously treated with both AS-NPs and JQ1-NPs or Rt-AS-NPs and Rt-JQ1-NPs. To account for any potential effects of chitosan or retinol on the cells, additional cells were treated with NPs or Rt-NPs at concentrations corresponding to the lowest and highest concentrations of drug-loaded NPs used in terms of polymer concentration. Cells treated with fresh cell culture media only served as the negative control. Four days after seeding, the cells were subjected to a second round of treatment, similar to the initial treatment. Three days after the second treatment, the cells were harvested. Cellular protein extracts were prepared using previously described methods [28], and Western blot analysis was performed under appropriate conditions. The equal loading of lanes was confirmed by probing the membrane with an antibody specific for glyceraldehyde 3-phosphate dehydrogenase (GAPDH), a housekeeping protein. Antibodies listed in Table 3, were used for the detection of specific proteins. Densitometric analysis was carried out to validate the Western blot results using LumiAnalyst software (version 3.1) and the Lumi-Imager system, both from Roche Diagnostics, Mannheim, Germany. Band intensities were normalized to the GAPDH signals, and the intensity of the control band was set to 1. The intensities of the other bands were expressed as relative density, allowing for comparison and quantification of protein expression levels.

Table 3. Antibodies used for Western blot analysis of fibronectin, vimentin and PDGFR-β expression.

Antibody	Cat. No	Company	Dilution	Clonality
Vimentin	EPR3776	Abcam, Amsterdam, The Netherlands	1:1000	r mAb
Fibronectin	AB1954	Sigma-Aldrich, Darmstadt, Germany	1:3000	r pAb
GAPDH (6C5)	sc-32233	Santa Cruz, Heidelberg, Germany	1:1000	m mAb
PDGFR-β (958)	sc-432	Santa Cruz, Heidelberg, Germany	1:1000	r pAb
β-actin	A5441	Sigma-Aldrich, Darmstadt, Germany	1:10,000	m mAb
goat anti-rabbit IgG (H+L), HRP	31460	Invitrogen, Waltham, MA, USA	1:5000	g
goat anti-mouse IgG (H+L), HRP	31430	Invitrogen, Waltham, MA, USA	1:5000	g

r, rabbit; m, mouse; g, goat; HRP, horse radish peroxidase; mAb, monoclonal antibody; pAb, polyclonal antibody.

2.8. Statistical Analysis

Tests were performed using Graph-Pad Prism version 9.2 (GraphPad Software, San Diego, CA, USA). Un-paired *t*-tests and ANOVA tests were performed followed by the Tukey post hoc test. Levels of statistical significance are indicated by asterisks; * $p < 0.05$, ** $p < 0.01$, *** $p < 0.001$ and **** $p < 0.0001$.

3. Results

3.1. Chitosan Nanoparticles Exhibit Easy Formulation, Tunable Functionalization and High Drug Loading Capacities

3.1.1. Chitosan NPs Characterization

The hydrodynamic diameter (HD) and zeta potential (ZP) of the NPs were determined from three independently prepared batches, resulting in average values of 129 ± 22 nm and 41 ± 1 mV, respectively. Figure 1 illustrates the characterization of the NPs, including (Figure 1B) a size distribution chart and (Figure 1C) SEM images. The SEM images reveal that the NPs exhibit a spherical morphology and the core sizes observed are in line with the hydrodynamic diameter measured using the Malvern Zetasizer instrument.

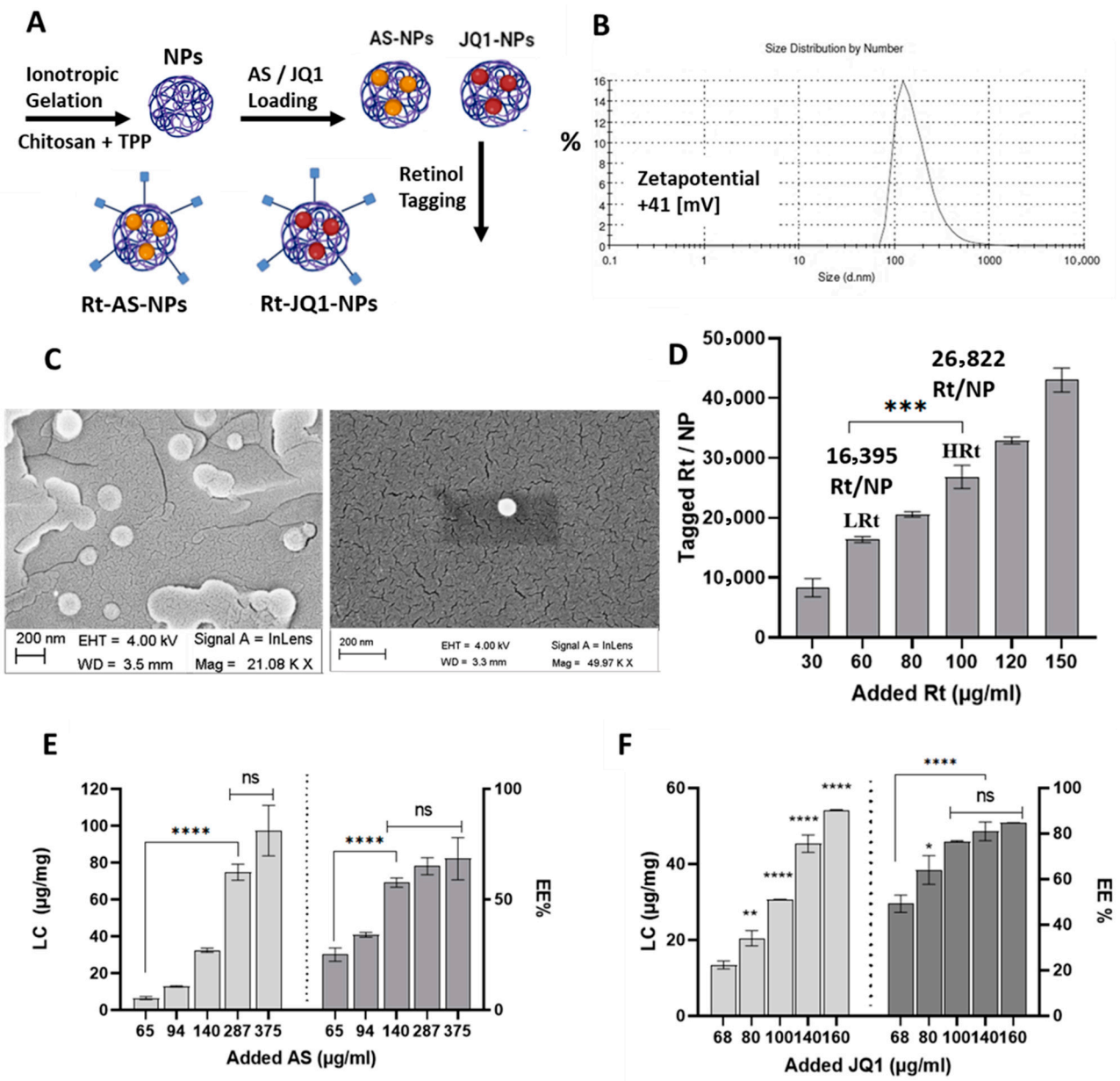


Figure 1. Nanoparticles formulation, characterization, functionalization and drug loading. (**A**) Ionotropic gelation preparation of NPs; (**B**) hydrodynamic diameter distribution characterization by Dynamic Light Scattering of plain unmodified NPs (n = 3); (**C**) scanning electron microscopy images of plain unmodified NPs (n = 3); (**D**) NPs modification with retinol (n = 3); and (**E**,**F**) quantification of unmodified chitosan NPs- atorvastatin and JQ1 loading capacities and EE% (n = 3). Statistical analysis was performed using GraphPad Prism version 9.2 (GraphPad Software, San Diego, CA, USA) with a one-way analysis of variance test (ANOVA), where (*) $p \leq 0.05$, (**) $p \leq 0.01$, (***) $p < 0.001$ and (****) $p < 0.0001$.

3.1.2. Modification of NPs with Retinol

By using the calibration curve presented in Figure A2A, derived from fluorometric analysis of a serial dilution of retinol ranging from 15 to 80 µg/mL at an excitation wavelength (ʎexc) of 335 nm and emission wavelength (ʎem) of 458 nm, we were able to quantify the concentration of retinol attached to the surface of NPs. As expected, increasing concentrations (30–150 µg/mL) led to a proportional increase in the tagged amount of retinol. Two specific concentrations, chosen to represent low and high retinol densities, were labeled as LRt-NPs and HRt-NPs, respectively. These concentrations corresponded to 16,395 and 26,822 retinol (Rt) molecules per NP (Figure 1D) or 0.23 and 0.38 Rt molecules

per square nanometer (nm^2) (Figure A2B). Retinol conjugation resulted in a slight increase in particle size; however, this increase was not significant. Additionally, a decrease in zeta potential was observed with the increasing tagged Rt. This decrease in NP positivity aligns with the consumption of chitosan amine group during conjugation (Table A2).

3.1.3. Determination of NPs Atorvastatin and JQ1 Loading Capacity and Encapsulation Efficiency (EE%)

Utilizing the calibration curve presented in Figure A3A, the right side of Figure 1E, displays the relationship between the added concentration of atorvastatin (AS) and encapsulation efficiency. The added concentration of AS ranges from 65 to 375 μg/mL, resulting in an increase in encapsulation efficiency (EE%) from 25%, 34%, 57%, 65%, up to 68%. Beyond an added AS concentration of 140 μg/mL, the EE% begins to plateau. However, it is important to highlight that the loading capacity showed a significant increase even at higher concentrations. On the left side of Figure 1E, the loading capacity (LC) varies from 6.5 to 97.5 μg per mg of NPs, indicating the amount of atorvastatin loaded per unit mass of NPs.

Similarly, using the calibration curve presented in Figures A3B and 1F illustrates the relationship between the added concentration of JQ1 and encapsulation efficiency. As the concentration of added JQ1 increased from 68 to 160 μg/mL, there was a gradual rise in encapsulation efficiency, ranging from 49% to 84%. Simultaneously, the amount of JQ1 loaded within the NPs also increased, from 13 to 54 μg/mg. It is important to note that while the encapsulation efficiency reaches a plateau, the loading capacity continues to rise.

3.2. Evaluation of the Impact of Retinol Tagging on GRX Cells Uptake Efficiency and Disease Targeting Ability

3.2.1. Evaluation of NP Uptake in GRX Cells

To evaluate the uptake of NPs, LRt-NPs, and HRt-NPs by GRX cells under varying conditions, including the presence or absence of excess retinol, a comparative analysis was conducted. Although, NPs showed the highest uptake level, it can be seen that HRt-NPs exhibited significantly greater uptake than their LRt counterparts. Intriguingly, when GRX cells were pre-treated with 7 mM retinol for 1 h before the uptake experiment, a substantial reduction in uptake was observed across all formulations, except for NPs (Figure 2B).

In order to assess the impact of collagenase pre-treatment on the uptake extent, GRX cells underwent treatment with 0.5 mg/mL collagenase encapsulated in NPs (Col-NPs), for a duration of 12 h. As anticipated from Figure 2C, the use of Col-NPs did not show any enhancement in uptake across all formulations.

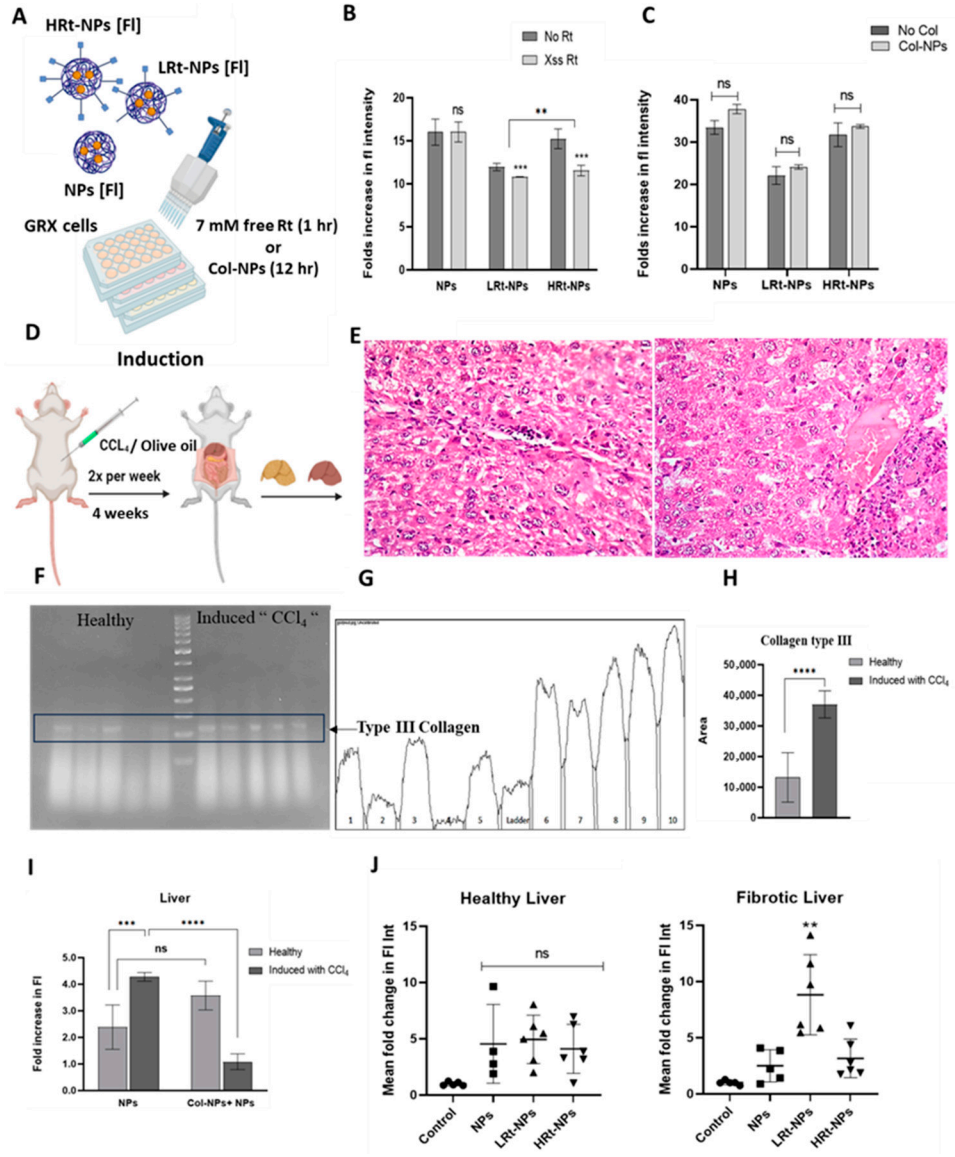


Figure 2. (**A**) Uptake experimental setup; (**B**) effect of retinol tagging on NPs uptake in GRX cells; (**C**) effect of collagenase pre-treatment on uptake of NPs, LRt-NPs and HRt-NPs by GRX cells; (**D**) induction of liver fibrosis in male Swiss albino mice using CCl_4 IP injections; (**E**) histopathological analysis of liver tissues of male Swiss albino mice after IP induction with CCl_4 using H&E stain; (**F**) Type III A1 collagen band separated by gel electrophoresis in the liver homogenates of healthy mice (**left**) and mice receiving IP injections of CCl_4 for 4 weeks (**right**); (**G**) area of each band; (**H**) quantification of type III A1 collagen in the liver homogenates of healthy mice and mice receiving IP injections of CCl_4 for 4 weeks; (**I**) in vivo evaluation of NPs passive accumulation in the livers; (**J**) biodistribution charts of NPs, LRt-NPs and HRt-NPs in the livers of healthy mice (**left**) and fibrotic mice (**right**). Statistical analysis was performed by GraphPad Prism version 9.2 (GraphPad Software, San Diego, CA, USA) using one-way analysis of variance test (ANOVA), where (**) $p \leq 0.01$, (***) $p < 0.001$ and (****) $p < 0.0001$.

3.2.2. Confirmation of Liver Fibrosis Induction

Examination of liver tissue from mice treated with intraperitoneal injections of CCl_4, as shown in Figure 2E, revealed discernible and characteristic features indicative of liver fibrosis. Images display frequent mitotic figures, with some nuclei showing chromatolysis and hyperchromasia, along with evidence of megahepatocytes, Kupffer cell proliferation, intranuclear vacuolation of hepatocytes, newly formed blood vessels containing coagulated red blood cells, severely dilated and engorged hepatic sinusoids, perivascular aggregation

of mononuclear inflammatory cells, and some enlarged hepatocytes exhibiting complete karyolysis of the nucleus and vacuolation of the cytoplasm.

3.2.3. Quantificationof Collagen Content in Liver Tissues of Healthy and Induced Mice

Figure 2F–H demonstrate the quantification of collagen type III within the liver tissue of both healthy mice and mice induced with CCl_4. The fibrotic group shows a 2.5-fold increase in collagen deposition compared to the control mice, as evidenced by the band areas.

3.2.4. NP Bio-Distribution

The study involved treating four distinct groups of mice with Fl-loaded NPs. To address potential interference from tissue autofluorescence, the accumulation of NPs in the liver was normalized as the fold change in fluorescence intensity relative to control mice within the same group. Figure 2I illustrates the accumulation of NPs in the livers, showing observable accumulation in both healthy and fibrotic mice. Furthermore, Figure 2I reveals noticeable differences when mice were pretreated with collagenase-loaded NPs before Fl-NPs injection. In healthy livers, collagenase treatment did not affect NP accumulation. However, in fibrotic livers, a significant reduction in NP accumulation was observed in the subgroup subjected to collagenase treatment.

Figure 2J illustrates the impact of retinol tagging on the accumulation of NPs in the livers of both healthy and fibrotic mice. An interesting observation is the increased accumulation of LRt-NPs in fibrotic livers, a trend not apparent in healthy livers.

It is noteworthy, that the retinol modification of the NPs exhibited no discernible impact on biodistribution, with NPs, LRt-NPs, and HRt-NPs showing no significant differences in the livers of healthy mice. Conversely, in fibrotic mice, LRt-NPs displayed the highest accumulation compared to NPs and HRt-NPs.

3.3. Evaluation of the Efficiency of Rt-NPs for Selective Hepatic Accumulation in Fibrotic Versus Healthy Mice

Figure 3A,B reveal differences when mice were pretreated with collagenase-loaded NPs before Fl-NPs injection. In healthy livers, accumulation did not increase with collagenase treatment. However, in fibrotic livers, a significant increase in LRt-NPs accumulation was observed in the fibrotic subgroup without collagenase.

Figure 3C,D depict the accumulation of NPs in the kidney homogenates. Both NPs and LRt-NPs exhibit higher accumulation in the kidneys of healthy mice compared to HRt-NPs. In the kidneys of animals treated with CCl_4, HRt-NPs also show lower accumulation. Collagenase pretreatment reduces the accumulation of NPs and LRt-NPs in the kidneys but does not affect that of HRt-NPs.

Figure 3E,F depict very minimal accumulation of all NP formulations in the brains of both healthy and fibrotic mice, regardless of collagenase pretreatment.

In Figure 3G,H, low NP accumulation is seen in the hearts of both healthy and fibrotic mice, with a similar trend to that observed in the kidneys, possibly due to collagen content in the heart.

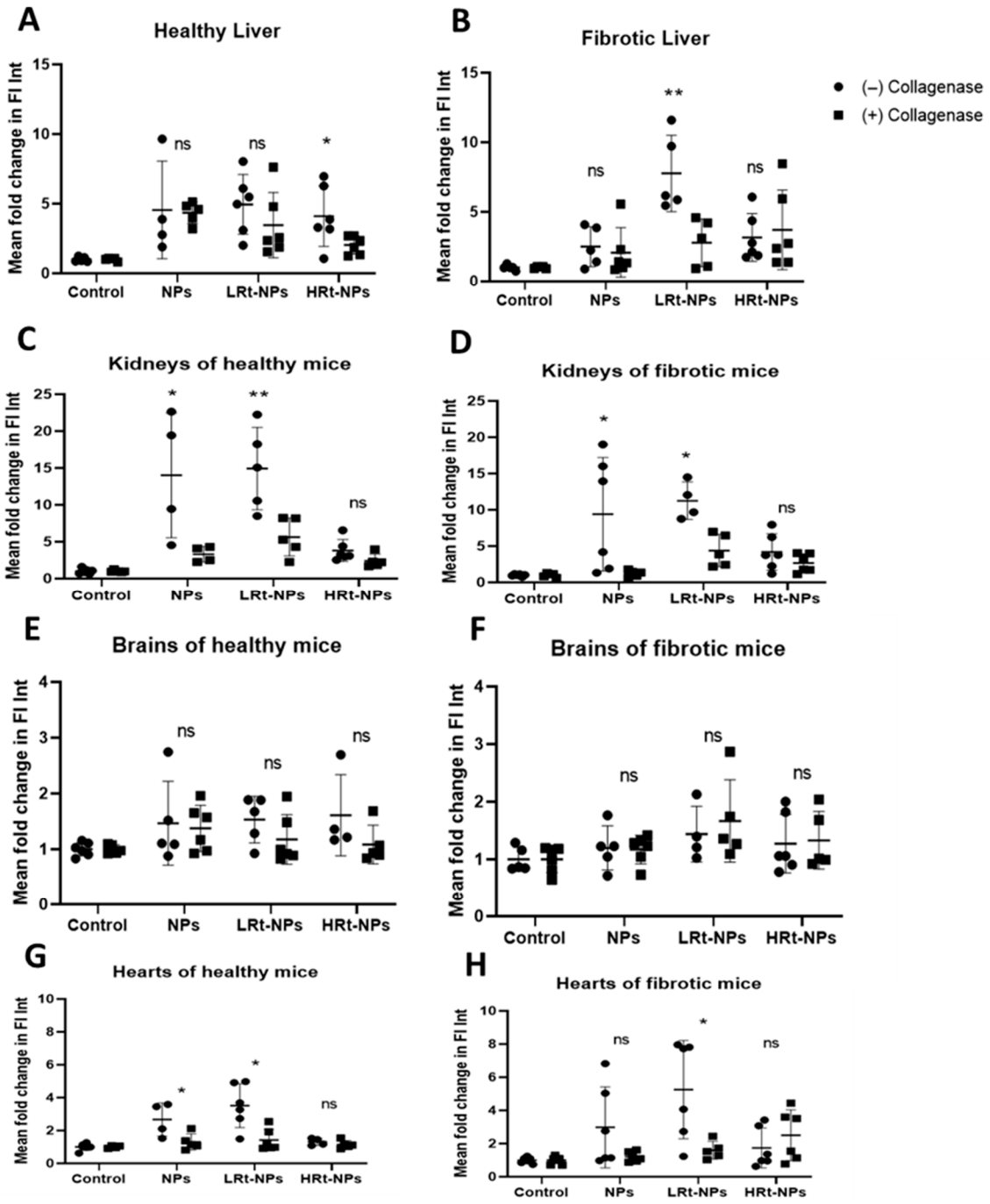


Figure 3. Biodistribution charts of NPs, LRt-NPs and HRt-NPs in (**A**) the livers of healthy mice; (**B**) the livers of fibrotic mice; (**C**) the kidneys of healthy mice; (**D**) the kidneys of fibrotic mice; (**E**) the brains of healthy mice; (**F**) the brains of fibrotic mice; (**G**) the hearts of healthy mice; and (**H**) the hearts of fibrotic mice. Mice were either untreated or pretreated with Col-NPs for a week before NPs administration. Statistical analysis was performed by GraphPad Prism version 9.2 (GraphPad Software, San Diego, CA, USA) using one-way analysis of variance test (ANOVA), where (*) $p \leq 0.05$ and (**) $p \leq 0.01$.

3.4. Assessment of the Ability of AS- and JQ1-Loaded Rt-Modified NPs to Deactivate aHSCs

3.4.1. Effect of AS- and JQ1-Loaded NPs on Cell Viability

Examining Figure 4A,B reveals the impact of various drugs and drug-loaded NPs on GRX cell viability, assessed through the MTT assay. In Figure 4A, escalating concentrations of JQ1, whether in its free molecular form or encapsulated in NPs or retinol-modified NPs, were investigated within the range of 2.5 to 30 μM. Notably, the percentage of viable cells

for JQ1-NPs dropped significantly below 60% at 25 µM. While comparing Rt-JQ1-NPs to their JQ1-NPs counterparts, a non-significant difference in viability was observed, except at 25 µM. In contrast, the JQ1 solution exhibited significantly lower viability across all concentrations range.

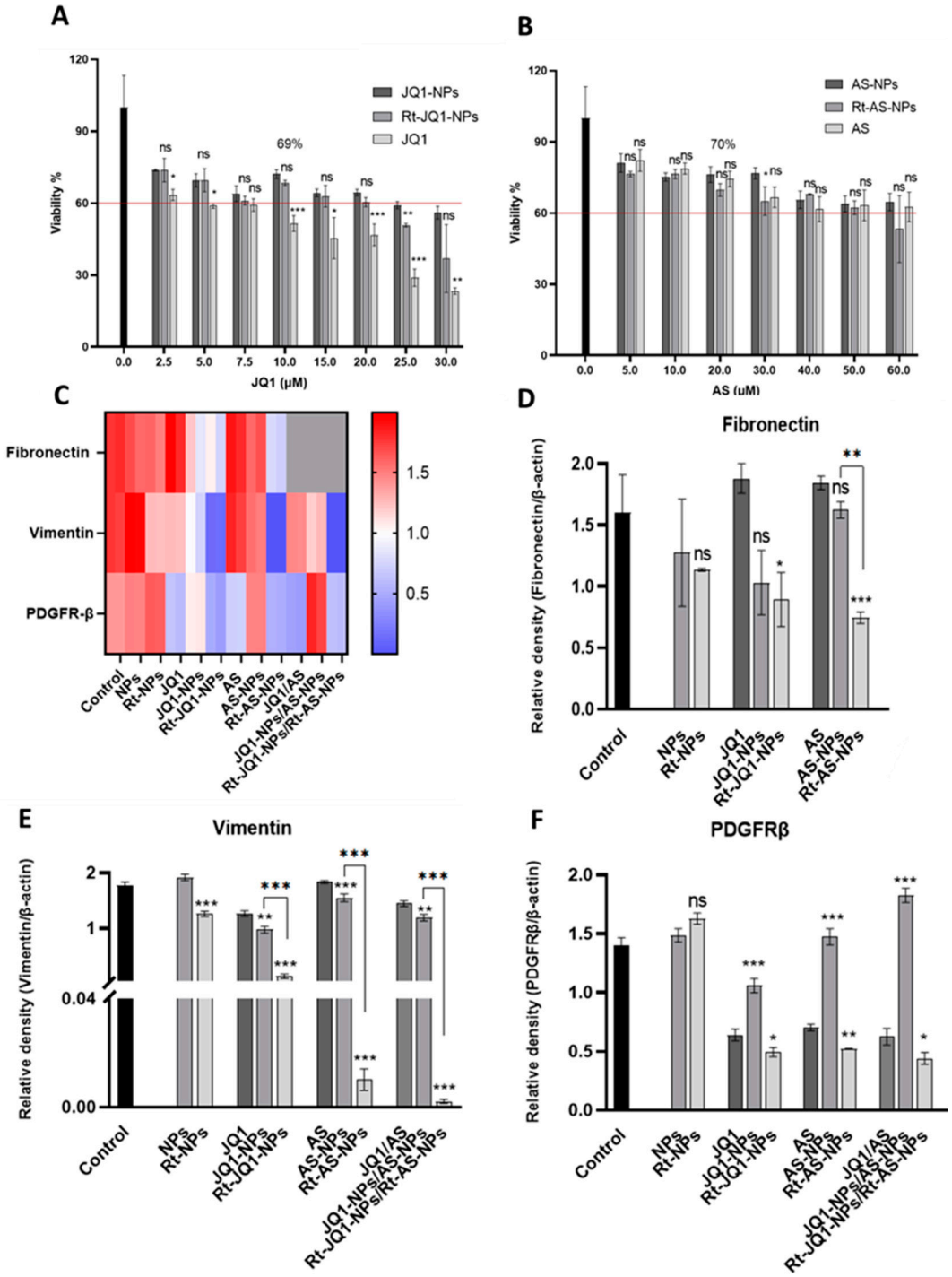


Figure 4. MTT assay of GRX cells treated with (**A**) JQ1, JQ1-NPs, and Rt-JQ1-NPs, and (**B**) AS, AS-NPs and Rt-AS-NPs, red line marks 60% cell viability. Assessment of the ability of JQ1 and AS to deactivate aHSC; (**C**) heat map showing levels of fibronectin, vimentin and PDGFR- β in cellular protein extracts of GRX cells after treatment with NPs. (**D**) Expression analysis of fibronectin, (**E**) expression of vimentin, and (**F**) expression of PDGFR-β using Western blot. Statistical analysis was performed by GraphPad Prism version 9.2 (GraphPad Software, San Diego, CA, USA) using one-way analysis of variance test (ANOVA), where (*) $p \leq 0.05$, (**) $p \leq 0.01$ and (***) $p < 0.001$.

Moving to Figure 4B, MTT assay results for AS-NPs, their retinol-modified counterparts, and AS in its molecular form were assessed at concentrations ranging from 5 to 60 μM. All formulations maintained viability above 60%, with no significant differences observed among the various formulations.

3.4.2. Assessment of the Ability of AS- and JQ1-Loaded NPs to Deactivate aHSCs

The deactivating potential of JQ1 and AS on GRX cells was assessed by examining the expression of three markers, presented as the relative density of the target to β-actin. Both drugs, in their molecular form or loaded into NPs or retinol-modified NPs (Rt-NPs), were tested at concentrations equivalent to 10 μM for JQ1 and 20 μM for AS. Figure A5 shows a representative replica of the Western blot analysis performed for the different markers. Figure 4C shows the heat map representing the expression of fibronectin, vimentin and PDGFR-β after GRX treatment with the different formulations.

In Figure 4D, the expression of fibronectin is depicted. The free forms of both drugs exhibited similar fibronectin expression compared to control untreated cells. JQ1-NPs and AS-NPs displayed a non-significant decrease in fibronectin expression, as did the co-treatment with both NPs. Notably, retinol-modified NPs showed a significant reduction in fibronectin expression, emphasizing their efficacy in modulating this marker.

Figure 4E illustrates the expression of vimentin. The free forms of the drugs, whether administered separately or as a co-treatment, did not alter vimentin expression compared to untreated cells. JQ1-NPs, AS-NPs, and co-treatment displayed a reduction in vimentin expression, with retinol-modified NPs exhibiting the most significant reduction. The co-treatment with retinol-modified NPs demonstrated an extremely significant reduction in vimentin expression.

Surprisingly, the expression of PDGFR-β, as shown in Figure 4F, yielded a different pattern. The free forms of JQ1 and AS led to a reduction in PDGFR-β expression, while JQ1-NPs, AS-NPs, and the co-treatment exhibited significantly higher expression, comparable to or even higher than control untreated cells. Nevertheless, the utilization of retinol-modified NPs led to a notable decrease in PDGFR-β expression. Interestingly, while the combined treatment exhibited a significant reduction in expression levels, it did not yield any additional effects compared to the individual treatment with either Rt-JQ1-NPs or Rt-AS-NPs.

4. Discussion

4.1. NP Formulation, Functionalization, Drug Loading and Chemical Characterization

Chitosan's selection in this study stems from its exceptional suitability as a carrier: a natural polysaccharide polymer derived from renewable sources through the deacetylation of chitin. It possesses several desirable attributes, including biodegradability [29], biocompatibility, minimal immunogenicity [30], and a hydrophilic nature driven by its abundance of amine and hydroxyl groups, which contribute to enhanced reticuloendothelial escapism, and inherent stealth properties. Additionally, the cationic nature of chitosan facilitates interactions with negatively charged cell membranes, promoting its internalization by targeted cells. The presence of numerous amine groups allows for diverse interactions with a wide range of ligands, enabling active targeting strategies. Moreover, chitosan has intrinsic collagen-binding properties, making it a suitable carrier for passively targeting collagen-rich organs such as fibrotic livers [31]. Given the fact that the liver sinusoidal endothelial cells fenestrae are organized in typical sieve plates and measure ≈ 50–250 nm in diameter [32]. However, in liver fibrosis, these endothelial cells undergo transformation leading to capillarization and loss of fenestrae. It is quite possible that highly fibrotic areas of the liver might not be readily accessible to NPs. Despite this, smaller NPs can still access

the space of Disse in areas where fenestrae remain accessible. Accordingly, in this study, NPs prepared were ≈130 nm in diameter to first enable evasion of RES sequestration, giving it a longer circulation time and to be able to access the space of Disse via the remaining fenestrae of the fibrotic liver.

Given that AS suffers from low water solubility (0.1 mg/mL), necessitating its exclusive oral administration and resulting in very low bioavailability (12%) [33]. Consequently, the encapsulation of AS within NPs presents novel avenues for alternative routes of administration, such as intravenous delivery, enhancing bioavailability. Similarly, the utility of JQ1 is limited by its off-target effects [34], as well as its short half-life and poor pharmacokinetic profile [35]. Therefore, encapsulating JQ1 within NPs shows promise in enhancing the efficacy of the treatment strategy, potentially reducing many of the adverse effects associated with systemic delivery. Importantly, chitosan NPs self-assembly through ionic gelation method eliminates the need for harsh conditions (such as heat or organic solvents) by forming NPs through electrostatic interactions between chitosan amines and a suitable cross-linker like sodium tripolyphosphate. This characteristic enhances its suitability as a carrier for the intended payloads.

In parallel, retinol has gained significant popularity as a ligand for targeting liver fibrosis. This is primarily because activated hepatic stellate cells (aHSC) preferentially and more efficiently take up retinol compared to their quiescent counterparts [18,19,36]. Additionally, retinol is less toxic than retinal and retinoic acid, making it the preferred choice [37]. Many scientists have specifically embraced retinol, as a targeting ligand for delivering various antifibrotic agents to HSCs.

However, the impact of Rt density on targeting efficiency has been a question, as previous articles often only used a single density of retinol-modified NPs. In that regard, we prepared NPs with two different Rt densities and importantly, the number of retinol molecules on HRt-NPs was significantly higher than that on LRt-NPs, demonstrating a substantial difference in retinol density between the two formulations. The selection of the LRt and HRt concentration was based on a thorough evaluation process involving multiple quantification studies. It was observed that concentrations lower than LRt approached the detection limit, making accurate quantification challenging. Conversely, concentrations higher than HRt led to NP aggregation due to the consumption of available amino groups in the tagging process.

4.2. Evaluation of the Impact of Retinol Modification on Cellular Uptake

To test the Rt density effect we utilized GRX cells, a continuous murine cell line that exhibits myofibroblast morphology. GRX cells exhibit an activated HSC phenotype, therefore they fit perfectly as our model system. These cells demonstrate the expression of extracellular matrix components, including thin fiber networks composed primarily of collagen I, III, IV, fibronectin, and laminin [38]. It is noteworthy that GRX cells express the retinol binding protein receptor in a manner similar to primary HSCs, further supporting their relevance as a model for activated HSCs in our investigation [39].

Interestingly, the significant reduction in the uptake extent upon retinol pretreatment suggests a potential insight into the uptake mechanism of retinol-modified NPs, indicating a highly specific process such as receptor-mediated endocytosis rather than a random or unspecific cellular engulfment. Several studies have confirmed the receptor-mediated uptake of retinol by HSCs [17,40]. Duong et al. demonstrated that unmodified NPs exhibited poor uptake compared to vitamin A-decorated NPs. Notably, this uptake significantly increased after cotreatment with retinol-binding protein, the carrier of vitamin A in the blood [20]. Indeed, there exists a reported correlation between Cellular Retinol-Binding Protein-1 (CRBP-1) expression and myofibroblastic differentiation. This observation is sub-

stantiated by the fact that during myofibroblastic differentiation, while hepatic stellate cells lose their retinol storage, they maintain a high level of CRBP-1 expression. Furthermore, in this process, portal fibroblasts acquire CRBP-1 expression [41].

Moreover, in the context of liver fibrosis induction through carbon tetrachloride, myofibroblastic alpha-smooth muscle actin (a-SMA)-positive HSCs were found to sustain CRBP-1 expression. Similarly, in models involving bile duct ligation, portal fibroblasts exhibited expression of both α-SMA and CRBP-1 [42]. Lepreux et al. discovered that the number of CRBP-1-positive HSCs increased with the progression of fibrosis [41]. These data elucidate the decreased uptake of LRt-NPs and HRt-NPs following pretreatment with retinol, as hypothesized based on the saturation of RBP with excess free retinol. However, since NPs still showed the highest uptake extent, it seems that this route is less dominant than the route utilized by unmodified NPs, unless NPs show cellular association as opposed to uptake. GRX are collagen producing cells, it therefore might be the case that unmodified NPs are adsorbing to collagen in the ECM and are not really being uptaken. For this reason, the experiment was repeated with collagenase-loaded NPs pretreatment.

Collagen, the most abundant protein in mammals and a primary component of the extracellular matrix, plays a crucial role in tissue maintenance, development, and regeneration under normal conditions. However, in pathological conditions such as arthritis, cancer, and fibrosis, there is an excessive production of ECM components. Specifically in fibrosis, activated HSCs produce an excessive ECM, characterized by collagen, proteoglycan, glycosaminoglycan, and glycoprotein [43]. This overproduction results from an imbalance between the processes of production and degradation, termed "remodeling".

In addressing fibrosis, the use of collagenase to digest the fibrotic scar and facilitate the accumulation of NPs in the liver has been explored. Given the short half-life of collagenase in the circulation, it was anticipated that collagenase-encapsulated NPs (Col-NPs) would provide higher protection compared to using free collagenase enzyme. To ensure the enzyme's protection from denaturation, we relied on loading collagenase into the NPs through electrostatic interaction between the negatively charged enzyme and the positively charged chitosan NPs, rather than a chemical reaction between them. This approach has also been employed by Luo et al. [44]. Moreover, it is noteworthy that collagenase is known for its high toxicity when administered intravenously. Therefore, the use of Col-NPs is expected to enhance the safety and tolerability of collagenase, providing a promising avenue for its therapeutic application.

We initially anticipated that co-treatment with Col-NPs would lead to a higher cellular uptake of NPs, whether unmodified or retinol-modified. However, intriguingly, our results did not align with these expectations. The observed inability of Col-NPs to enhance NP uptake could be attributed to the slow release of collagenase from the sustained release system. There is a plausible hypothesis that the duration of the 12 h pre-treatment may not be sufficient to induce a significant release of collagenase from the NPs, leading to a decrease in the extracellular matrix produced by GRX cells. This hypothesis is supported by previous studies conducted by our research group, which demonstrated that the release of fluorescein, used as a model drug within the same NP system, did not exhibit any significant release of the dye over a 24 h testing period. It should be noted that fluorescein is a smaller and more hydrophilic molecule compared to collagenase, suggesting that it would exhibit a faster and more pronounced burst release compared to the larger-molecular-weight collagenase enzyme [24].

4.3. Evaluation of the Effect of Retinol Tagging on NP Bio-Distribution

In vivo, liver fibrosis models can be categorized into five types based on their causes: chemical, dietary, surgical, transgenic, and immune. Among these, chemical injury-induced

models are the most commonly utilized. These models involve the administration of chemical drugs that enter hepatocytes and produce toxic metabolites, leading to persistent liver injury and the development of fibrosis [45].

The use of CCl_4 as a liver fibrosis inducer in animal models has gained significant acceptance and demonstrated its efficacy, as supported by numerous studies, including those conducted by our own research group [25,26]. CCl_4-induced intoxication in rats leads to severe hepatic injury, resembling acute hepatitis exhibiting symptoms similar to those observed in humans; moreover, it resembles human liver fibrosis in terms of morphology and pathophysiology, making it highly valuable for research purposes [46]. Specifically, the utilization of this particular protocol for liver fibrosis induction has proven to be optimal, as it involves a dosing regimen of two injections per week. This dosage regimen has shown superior outcomes in terms of reproducibility of fibrosis induction and the timely generation of fibrosis/cirrhosis, when compared to lower levels of inducer exposure [47]. In addition to offering several advantages, including low development costs, a straightforward implementation method, a short induction period, and significant pathological changes in liver tissue. Furthermore, after discontinuation of drug administration, the pathological alterations in the liver can be reversed. Consequently, the CCl_4-induced fibrosis model is considered representative and highly reproducible, making it a preferred choice for studying liver fibrosis development and investigating mechanisms of liver repair [48]. The significant changes observed in the histopathological examination, together with the marked increase in collagen type III expression, clearly confirm that our model successfully induced liver fibrosis. This increase in collagen expression is consistent with previously reported findings in liver fibrosis models.

In normal livers, collagen types I, III, and V are typically present [49]. Numerous studies have highlighted the escalated deposition of fibrillar collagens I and III following chronic liver injury [50]. Additionally, the expression of ECM proteins is believed to surge approximately 8–10 times in fibrotic conditions. This process typically initiates with heightened expression of fibronectin cellular isoforms in the space of Disse, followed by increased levels of collagens I, III, and IV, alongside the emergence of laminin [51,52]. Moreover, Karsdal et al. have reported that a cirrhotic liver contains roughly four times the amount of type III collagen compared to a healthy liver [49]. Likewise, augmented collagen deposition was observed in mouse models induced with CCl_4 [53,54].

After the successful induction, the differences in nanoparticle uptake observed in GRX cells following retinol modification prompted us to investigate whether a similar pattern would occur in vivo. As an initial step, however, we aimed to assess the ability of unmodified nanoparticles to accumulate in the fibrotic liver.

The observed accumulation in the livers of both healthy and fibrotic mice could be attributed to the organ's high vascularity and substantial blood volume even in healthy subjects. A notable finding is the marked increase in NP accumulation within fibrotic livers. Chitosan NPs [55] or chitosan-coated NPs [56] have become popular carriers for anti-fibrotic drugs and have been widely used by many researchers. Our research group has previously reported similar enhanced NP accumulation in fibrotic livers [25,26,31]. This phenomenon can be attributed to the inherent ability of chitosan to interact with augmented collagen deposition through hydrogen bonding [57], as previously demonstrated by our research group [26,31].

Considering that fibrosis involves excessive deposition of extracellular matrix, particularly collagen, it would be advantageous to investigate the potential benefits of pretreating animals with collagenase and assessing its impact on the accumulation of NPs in the target organ. However, it has been extensively documented that the intravenous administration of free collagenase can lead to lethal outcomes [26], primarily due to the occurrence of

hemorrhagic side effects [58]. In light of these findings, the encapsulation of collagenase within NPs has been demonstrated to enhance the safety and tolerability of the enzyme. Collagenase itself has demonstrated promising potential as an anti-fibrotic agent [59,60], particularly following its approval by regulatory bodies such as the FDA and EMA for the treatment of palmar fibromatosis (Dupuytren's contracture) [61]. However, its direct therapeutic application systemically is limited due to its short in vivo half-life and physical and chemical instability. Due to the presence of tissue proteases and its susceptibility to rapid proteolysis, as well as its vulnerability to denaturation caused by oxidation, hydrolysis, and other factors [61]. The inherent instability of collagenase renders it susceptible to complete loss of activity within a brief period of time. Notably, collagenase exhibits a short serum half-life ranging from 6 to 30 min [62]. To overcome the aforementioned challenges, as discussed above, the encapsulation of collagenase into chitosan NPs was chosen as a strategy. Chitosan NPs offer several advantages for delivering collagenase, as their encapsulation process occurs under mild conditions without the need for heat or organic solvents. Extensive studies conducted by our research group in earlier work focused on investigating the procedure for encapsulating collagenase into chitosan NPs while preserving its activity [26]. Moreover, this encapsulation strategy enables controlled release of collagenase, facilitating prolonged enzymatic activity within the target tissues. Extending the half-life and maintaining an effective concentration of collagenase in circulation, provides a means to enhance its therapeutic efficacy and prolong its impact on the target tissue, consequently, mitigating the need for frequent and repetitive dosing [61].

In that sense, the decreased accumulation of NPs in the livers of fibrotic mice but not the healthy mice following pretreatment with Col-NPs can be explained by the therapeutic potential of collagenase and the ability of Col-NPs to release their collagenase payload in an active form capable of degrading excessive collagen deposition. Previous studies conducted by our research group [26] have shown the ability of collagenase injection to reverse liver fibrosis. Additionally, Jin et al. reported the reversibility of liver cirrhosis in rabbits through portal collagenase perfusions [59]. Moreover, Lin et al. documented the therapeutic efficacy of collagenase treatment in rabbits with oral submucous fibrosis, providing further evidence of the positive therapeutic effect of collagenase in fibrotic conditions [63].

Interestingly, the increased accumulation of retinol-modified NPs in the fibrotic livers, an observation that was not noticed in the livers of healthy mice, could be attributed to the higher number of activated HSCs present in existing fibrosis and their robust proliferation. It is estimated that HSCs proliferate by 10–20 times during the progression of fibrosis [22]. The ongoing transformation of cells into activated HSCs in the dynamic process of liver fibrogenesis may also be a contributing factor, considering that activated HSCs demonstrate a greater propensity for retinol uptake compared to quiescent HSCs, as explained earlier [19]. On another hand, the preferential accumulation of LRt-NPs in the fibrotic organ can be attributed to the abundance of the retinol binding protein receptor, affirming that active targeting synergizes with passive targeting, imparting greater specificity to systemic treatment modules and minimizing undesired systemic side effects. Moreover, the preferential accumulation of LRt-NPs over HRt-NPs underscores the critical role of optimum ligand density for successful targeting in the desired organ. Since HRt-NPs exhibit lower accumulation than LRt-NPs, it indicates that our system adheres to the principle of optimum ligand density at its maximum, as elucidated by Alkilany et al. [64]. Several studies have reported that lower density of the targeting ligand often yields superior accumulation or therapeutic efficacy, irrespective of the NP nature or the disease context [65,66]. Our research group has reported similar observations, where El-Safy et al. found that chitosan NPs with low collagen binding peptide density exhibited enhanced efficacy in treating liver fibrosis, and

Tammam et al. reported that an intermediate density of the nuclear localization sequence on chitosan NPs resulted in the highest nuclear localization [26,67].

While higher ligand density might contribute to increased accumulation, it can also lead to downregulation of the desired receptor or steric hindrance that impedes the ligand from binding to the receptor initially. This phenomenon arises when molecules in close proximity adopt non-optimal orientations for binding [68]. Hence, researchers should exercise caution and optimize each system individually. Alkilany et al. conducted a study aiming to examine the impact of escalating targeting ligand density on NP-cellular interactions in vitro. Intriguingly, their findings revealed that augmenting ligand density does not consistently lead to heightened cell internalization. Instead, the results demonstrated the occurrence of a plateau or even a decrease in cellular uptake with increasing ligand density [64].

This effect is particularly accentuated in the case of Rt, given that the uptake by HSCs predominantly occurs through an intermediate complex where Rt binds to retinol-binding protein (RBP) as indicated earlier [17]. RBP is a relatively small protein (21 kDa) characterized by a beta-barrel cavity utilized for Rt binding. During Rt binding, the hydrophobic portion of Rt is ensconced within this cavity, while the hydroxyl group of Rt is exposed on the protein surface [69]. These hydroxyl groups were employed to conjugate Rt to the surface of chitosan NPs. Consequently, the spatial arrangement between the hydrophobic regions of Rt molecules must allow ample room for RBP binding [25].

It is noteworthy that, although Rt tagging of NPs enhanced cellular uptake in vitro and increased tissue accumulation in vivo, the optimal Rt density differed between the two settings. This discrepancy underscores the limitations of in vitro experiments in fully predicting in vivo behavior, a phenomenon we previously examined [24] and that has also been reported by others. For example, Pan et al. observed no significant enhancement in cellular uptake of Rt-NPs in vitro, yet his in vivo studies demonstrated pronounced liver accumulation within 15 min post-administration [22]. These findings highlight the importance of advancing to more complex, dynamic in vivo models prior to translation into clinical trials. Owing to this discrepancy, subsequent experiments were performed using LRt-NPs, hereafter referred to as Rt-NPs.

Additionally, the significant increase in LRt-NPs accumulation in the livers of the fibrotic subgroup without collagenase, while no impact for collagenase pre-treatment in the healthy subgroup, could be attributed to the therapeutic potential of collagenase as above mentioned. In previous work from our groups [26], we have shown that collagenase injection has the capacity to reverse liver fibrosis. Although the ability of collagenase injections to deactivate aHSCs and down-regulate retinol receptor expression has not been demonstrated. It is possible that a reverse in activation by collagenase and the resultant reduction in retinol receptor would result in a decrease in LRt-NPs accumulation such as the case seen in fibrotic livers.

The significant accumulation of NPs in the kidneys, though unintended, is understandable and has been reported by other research groups [20]. This accumulation could be attributed to secondary kidney dysfunction as a complication of liver fibrosis, known as hepatorenal dysfunction [70], considering that kidneys are the main organs of elimination and have high blood flow. However, this would not explain why the same accumulation trend and amount were observed in healthy animals that did not receive CCl_4. Another possible explanation is the presence of receptors capable of binding to retinol, such as retinoic acid receptors (RARα, β, and γ) in mesangial cells, podocytes, and proximal tubule epithelial cells [71]. Additionally, the kidneys are one of the main organs containing large amounts of collagen [72]. Since chitosan NPs bind to collagen [26,57] and unmodified NPs and LRt-NPs have a higher surface area of exposed chitosan compared to HRt-NPs where

the chitosan surface is shielded by retinol, it is plausible that they exhibit high accumulation. If collagen is digested by collagenase, then this accumulation is reduced. The accumulation of all tested NPs in the kidneys showed variability among mice within the same group. Some mice displayed minimal accumulation, while others showed significantly higher levels, contributing to fluctuations in the mean values.

The accumulation observed in the brains, although minimal could be due to the well-known ability of chitosan to cross the blood–brain barrier (BBB) [73], this ability is attributed to potential ionic interactions between NPs and endothelial cells, leading to adsorptive-mediated transcytosis, as reported by Caprifico et al. [74]. Similarly, Wang et al. observed significant accumulation of chitosan-coated NPs in various brain regions in mice, including the cortex, paracoele, third ventricle, and choroid plexus epithelium [75]. Jahromi et al. also noted similar accumulation of chitosan NPs in rat brains [76]. It is worth noting that the particles used in these studies shared similar size and positive zeta potential with the NPs in our study.

The minimal accumulation observed in the heart is as well understandable, since the heart contains a significant amount of type I and III collagen, which are crucial for its structural integrity and function [77]. However, comparing NP accumulation in the liver to the main tested organs (heart, brain, and kidneys) reveals a clear pattern. The liver shows higher, more consistent, and specific accumulation compared to other organs, indicating the success of our system in targeting the organ of interest and reducing systemic side effects. Our biodistribution findings align with previous reports demonstrating similar distribution patterns. Duong et al. reported preferential accumulation of vitamin A-decorated NPs in the livers of bile duct ligation rats compared to healthy controls, with greater accumulation in the liver than other organs [20]. Qiao et al. found higher accumulation of vitamin A-decorated micelles in the livers of fibrotic mice compared to healthy mice, with greater accumulation in the liver than in kidneys, spleen, heart, and lungs [78]. Including retinol in any form seems to enhance hepatic NP accumulation, as Pan et al. demonstrated higher hepatic accumulation of retinol-loaded lipid nanocarriers compared to retinol-free counterparts [22].

4.4. Assessment of the Safety of Drug-Loaded NPs and Their Ability to Deactivate aHSCs

Before investigating the potential of drug-loaded nanoparticles to deactivate aHSCs, we first aimed to ensure the safety of the nanoparticles and the tolerability of the drugs at the selected doses. This was essential to confirm that any observed decrease in the analyzed markers expression would be a direct result of the drug's effect rather than cell death. Therefore, we tested increasing concentrations of drug-loaded nanoparticles and their retinol-modified counterparts, alongside the corresponding free drugs.

The observed decline in percentage viability with increasing concentrations of JQ1 is consistent with its known anti-proliferative properties. JQ1, recognized for its anti-proliferative effects, has been extensively investigated as an anti-tumor agent in various cancer types, including triple-negative breast cancer and bladder cancer cells [79–81]. However, incorporating JQ1 into NPs serves to enhance its safety profile. Chitosan, employed as the biocompatible polymer for encapsulation, demonstrates a well-established safety profile in both in vitro and in vivo studies. Loading JQ1 into NPs not only increases safety, but based on the reported encapsulation efficiency, enables the use of higher drug amounts without encountering potential toxic side effects. Contrary to previous findings by Celano et al. and Maggisano et al., where JQ1-NPs exhibited significantly higher cytotoxicity compared to free JQ1, our MTT assay results indicate that both JQ1-NPs and Rt-JQ1-NPs display significantly higher cell viability. Noteworthy, Celano et al. reported 50% cell viability in MDA-MB 231 and MDA-MB 157 when using 0.06 μM of JQ1-loaded Zein NPs,

while Maggisano et al. observed 50% cell viability at 0.05 μM in MDA-MB-231 and 0.5 μM in MDA-MB-157 of JQ1-PLGA NPs. In the current study, chitosan NPs demonstrated 56% viability at a much higher drug concentration of 30 μM. Even when the particles were decorated with retinol, Rt-JQ1-NPs exhibited 50.8% at 25 μM drug concentration in GRX cells [80,81].

Atorvastatin, the FDA-approved HMG CoA reductase inhibitor, has garnered widespread attention for its compelling outcomes as an anti-inflammatory, anti-tumor, and anti-fibrotic agent. The repositioning of this extensively used drug not only circumvents the need for prolonged safety tests but also spares numerous animal lives, expediting the availability of a beneficial therapeutic for a multitude of patients. The limited aqueous solubility of AS (0.1 mg/mL), necessitating its exclusive oral administration and resulting in very low bioavailability (12%) [33] has constrained its application in intravenous injection formulations. By encapsulating atorvastatin within NPs, we not only gain the advantage of a targeted dosage form but also create a platform for exploring new routes of administration enhancing the drug bioavailability. This innovative approach not only enhances the drug's effectiveness but also opens avenues for expanding its use in novel therapeutic modalities. Ensuring the safety of NPs was paramount, and the graph illustrates that incorporating the drug into the NPs did not alter the percentage viability of GRX cells significantly. Despite a slight drop in viability observed at 40 μM, even at the highest concentration tested (60 μM), both AS-NPs and Rt-AS-NPs displayed a high safety profile, maintaining around 70% viability.

In comparison, Sarbassova et al. studied the effect of increasing AS concentration on five different cancer cell lines over 24 h. Notably, the observed viabilities varied across cell lines, with some showing significant drops (30% at 100 μM AS) [82]. Haidar et al. also investigated the effect of AS, AS-NPs, and plain chitosan NPs on cell viability in L-929 and B35 cell lines. After 24 h of exposure, all three formulations showed similar viability percentages. However, after 48 h, differences started to emerge. In L-929 cells, AS-NPs exhibited higher viability percentages than plain NPs in a concentration-dependent manner. In fact, AS-NPs even showed higher viability percentages than the free AS solution at 10 μM, surpassing the viability of untreated control cells. In B35 cells, AS-NPs also had higher viability percentages than plain NPs. However, when compared to the AS solution, not only did AS-NPs exhibit higher viability percentages than the control, but the AS solution itself started to show toxicity in a concentration-dependent manner. The authors attributed the higher viability of AS-NPs to the positive impact of chitosan on cell proliferation [83].

Considering the insights gained from previous research, we selected concentrations equivalent to 10 μM and 20 μM of JQ1 and AS, respectively, for further experiments with drug-loaded NPs and their retinol-modified counterparts. Consequently, assessing the safety profile of the combination therapy was crucial before proceeding with the therapy experiment. Figure A4 illustrates the percentage viability of co-treatments involving AS-NPs/JQ1-NPs, Rt-AS-NPs/Rt-JQ1-NPs, and AS/JQ1, compared to an equal amount of drug-free NPs or Rt-NPs. Notably, drug-loaded NPs exhibited lower viability compared to their plain NPs counterparts. This could be attributed to the chemopreventive and anti-proliferative potential of both AS and JQ1 [79–82]. However, the free drug solutions combination demonstrated significantly lower viability relative to the combination of drug-loaded NPs or the retinol-modified NPs. Specifically, AS-NPs/JQ1-NPs and Rt-AS-NPs/Rt-JQ1-NPs demonstrated 82% and 59% viability, respectively, compared to the combined free drugs (AS/JQ1) (49.6%). This highlights the enhanced safety profile conferred by encapsulating the drug into NPs. Detailed viability percentages are stated in Table A3.

As previously noted, the activation of HSCs is linked to cytoskeleton remodeling. This process provides the necessary framework for coordinated cellular movement and division, facilitated by the ability of cells to extend protrusions, establish adhesions at the leading edge, translocate the cell body, and ultimately detach from the substrate [84]. Several factors have been identified as contributors to the cytoskeleton remodeling process. Among them, fibronectin stands out, a multifunctional glycoprotein synthesized by fibroblasts, endothelial cells, macrophages, and hepatocytes. Found in the extracellular matrix, cell membrane, and cytoplasm, fibronectin plays a crucial role in collagen matrix assembly. Additionally, it is involved in cell proliferation, adhesion, and cell cycle progression. Previous studies indicate that increased expression of fibronectin isoforms EIIIA and EIIIB is associated with wound healing and tissue repair. Notably, heightened EIIIA expression has been implicated in the conversion of lipocytes to myofibroblasts in human hepatic fibrosis [85]. Moreover, it has been observed that excessive fibronectin deposition precedes collagen deposition, underscoring the pivotal role of fibronectin in the progression of fibrosis [86]. Furthermore, Altrock et al. reported that the use of inhibitors targeting fibronectin matrix formation led to a reduction in the progression of fibrosis and an improvement in liver function [87]. Liu et al. conducted comprehensive investigations on fibronectin expression, both in vitro using HSC-T6 immortalized rat cells and in vivo using Wistar rats. Their findings revealed that the level of fibronectin expression is not only linked to the nature of fibrosis, whether acute or chronic, but also exhibits an increase in a time-dependent or stimulant dose-dependent manner. This association underscores the potential of fibronectin as a valuable marker for assessing the degree of hepatic fibrosis [86]. Attallah et al. went a step further by devising a diagnostic predictive index value termed the fibronectin discriminant score (FDS). This innovative score, incorporating fibronectin along with APRI (Aspartate Aminotransferase to Platelet Ratio Index) and albumin, was established through assessments on 325 patients across various degrees of fibrosis. Their conclusion emphasized the superior efficiency of fibronectin among all the tested parameters. As a result, they proposed fibronectin as a direct marker, advocating for its use to replace invasive biopsy procedures in distinguishing patients with significant liver fibrosis from those with minimal liver fibrosis [88].

Given the pivotal role of HSC migration in liver fibrogenesis, inhibiting this cellular process holds significant promise for suppressing the progression of the disease [89]. Therefore, vimentin assumes considerable importance and merits comprehensive study. As a major protein within the intermediate filament protein family, vimentin plays a crucial role in stabilizing focal adhesions a process essential for the regulation of cell migration [90]. Vimentin is acknowledged as a hallmark of epithelial–mesenchymal transition [84]. Additionally, vimentin networks play a regulatory role in integrin mediated cell adhesion and contribute to directed cell movement through a highly intricate phosphorylation pattern. The specific sites and kinases involved in this pattern correspond to different cellular states, including mitosis, differentiation, and stress. These factors collectively govern the assembly and structure of cellular filaments [91]. Furthermore, vimentin functions as a signal transducer, conveying messages from the extracellular matrix to the cell nuclei [92]. Moreover, the absence of vimentin results in impaired wound healing, attributed to deficiencies in the migratory capacity of fibroblasts [91]. Numerous articles have documented the overexpression of vimentin in fibrotic diseases. Wang et al. reported an increased expression of vimentin in a time-dependent manner in rats treated with dimethylnitrosamine (DMN). Similarly, they observed elevated vimentin expression in patients with hepatic fibrosis compared to controls in a cohort study, emphasizing the clinicopathological significance of vimentin. To further establish its role at the molecular level, the group demonstrated delayed wound healing after the knockdown of vimentin in HSC-T6 cells. Notably, this delay indicated suppressed invasive and migratory abilities of HSCs. Additionally, the study

reported marked reductions in other cytoskeletal proteins, including filamin, α-actinin, plectin, talin, and vinculin, highlighting the role of vimentin as a modulator for other cytoskeleton proteins [84]. Furthermore, in a random forest analysis, Wang et al. identified vimentin as the most significant gene among all the studied Differentially Expressed Genes (DEGs) in TLR-4 and LPS challenge models for predicting advanced liver fibrosis. The study demonstrated consistently upregulated levels of vimentin in various liver diseases, including cirrhosis, liver failure, chronic hepatitis B, and fatty liver disease, as well as in liver injury models such as BDL, CCl_4, and DMN [93].

On another hand, numerous growth factors and their associated signaling pathways have been documented to contribute to fibrosis by modulating fibroblast activation, inducing apoptosis in epithelial cells, and orchestrating processes such as epithelial–mesenchymal transition (EMT) and endothelial–mesenchymal transition (EndMT). One prominent factor within this context is the platelet-derived growth factor (PDGF) and its corresponding receptors, PDGFR [94]. Under normal physiological conditions, the α granules of platelets primarily express PDGF. However, in response to liver damage or injury, the expression of PDGF is significantly upregulated in macrophages, injured endothelial cells, and activated HSCs [95]. Similarly, the expression of PDGF receptors is normally restricted to arterial vascular smooth muscle cells (VSMC), portal fibroblasts, and hepatic stellate cells in healthy livers [96]. It is noteworthy that PDGFRs are tyrosine kinase receptors, existing in two variants: PDGFR-alpha (PDGFRα) expressed by HSCs, and PDGFR-beta (PDGFRβ), whose expression increases during HSC activation [97]. Both PDGFR α and PDGFR β consist of five structural domains: an immunoglobulin-like domain, transmembrane domain, ATP binding site, intracellular hydrophilic kinase insert domain, and cytoplasmic tail [95]. Upon binding of different PDGF isoforms to their respective receptors, the receptors undergo dimerization, leading to phosphorylation of tyrosine residues at the intracellular domain and activation of various profibrogenic cascades through downstream signals (RAS/MAPK, PI3K/AKT, and JAK/STAT pathways) [98]. In the early stages of chronic liver damage, there is an increase in the expression of both receptors, with PDGFR-α being produced by myofibroblasts in fibrous septa and regenerative hepatocytes, while PDGFR-β is exclusively expressed in pro-fibrotic myofibroblasts [96]. Additionally, through autocrine mechanisms, the synthesized PDGF activates HSCs. Both of these events enhance cellular chemotaxis and decrease the intracellular amount of vitamin A [95]. Numerous researchers have delved into the examination of PDGFR behavior at various levels. For instance, Borkham-Kamphorst et al. reported that treating primary rat myofibroblasts with PDGF-B and PDGF-D leads to PDGFR-β autophosphorylation, activating downstream signaling molecules such as ERK1/2, JNK, p38 MAPK, and PKB/Akt, inducing robust mitogenic and pro-fibrotic responses in the cells. They observed upregulation of both variants of the receptor and all isoforms of PDGF in a rodent model of bile duct ligation as well [99]. As a result, the manipulation of PDGF and PDGFR has become a focal point of many studies. For instance, Kocabavoglu et al. induced the activation of PDGFR-β in HSCs in transgenic mice, leading to the activation of HSCs and myofibroblasts, ultimately causing the development of liver fibrosis [97]. The receptor was also upregulated in mice treated with CCl_4 [98]. Conversely, the downregulation or silencing of the receptor has been shown to attenuate liver fibrosis [96]. Furthermore, at a clinical level, the livers of fibrosis/cirrhosis patients exhibit an increased expression of PDGFR-β. Additionally, the soluble form of the receptor, sPDGFR-β, is elevated in patients with liver fibrosis and is correlated with the degree of fibrosis. This correlation allows for the differentiation of patients with minimal fibrosis (F0-1) from those with significant fibrosis ($F \geq 2$). Importantly, this diagnostic utility is independent of the underlying etiology of the disease, highlighting PDGFR-β as a straightforward and effective diagnostic tool [98].

After demonstrating the crucial role of fibronectin, vimentin and PDGFR-β in activating HSCs and their connection to the advancement of fibrosis and disease severity, it is important to note that the substantial decrease in the expression of all markers highlights the potential of combination therapy with Rt-AS-NPs and Rt-JQ1-NPs in treating liver fibrosis. Several studies have shown the effectiveness of statins in reducing fibronectin levels in conditions such as lung fibrosis [100,101] and diabetic nephropathy [102]. Atorvastatin has been shown to reduce vimentin upregulation in lung cancer [103] and viral infections like HIV or Zika virus [104]. Additionally, atorvastatin can suppress the PDGFR-β-Akt signaling pathway, inhibiting abnormal proliferation of vascular smooth muscle cells in atherosclerosis and restenosis [105], as well as decrease PDGFR-β expression in a rat model of non-alcoholic steatohepatitis (NASH) [106]. Similarly, JQ1 has also shown efficacy in reducing fibronectin expression in peritoneal damage associated with end-stage kidney disease [107] and corneal scarring [11]. JQ1 has demonstrated efficacy in lowering vimentin expression in gastric cancer [108], peritoneal damage [107], and salivary adenoid cystic carcinoma [109], as well as downregulating PDGFR-β expression in melanoma [110] and renal fibrosis [111]. Moreover, Wendler et al. have shown that deleting the retinol-binding protein gene in mice leads to decreased serum retinol levels and increased fibronectin deposition [112], while vimentin can be downregulated by nuclear retinoid X receptor agonists [113]. Manku et al. demonstrated an interaction between retinoic acid and PDGF receptor signaling in regulating neonatal gonocyte and embryonal carcinoma cell differentiation [114]. The evidence supports the potential effects of combination therapy, particularly using retinol-modified NPs. It is important to note that most studies on the effects of AS, JQ1, and retinoids on inhibiting or downregulating fibronectin, vimentin, and PDGFR-β have been conducted in oncological contexts. By establishing the critical roles of fibronectin, vimentin, and PDGFR-β in HSC activation and their direct link to fibrosis progression and disease severity, the significant reductions observed in these markers emphasize the therapeutic potential of combination therapy with Rt-AS-NPs and Rt-JQ1-NPs in treating liver fibrosis.

4.5. Limitations

Although encapsulation efficiencies were thoroughly assessed and our previous work provides an overview of the sustained release characteristics of the nanoparticles, the detailed release profiles of the encapsulated drugs were not evaluated in this study. Additionally, while the in vitro findings clearly demonstrate the potential of drug-loaded nanoparticles to deactivate activated hepatic stellate cells, further in vivo investigations are required to confirm and validate these effects in a physiologically relevant setting.

5. Conclusions

The introduction of retinol on NP surface enhances their specificity and targeting capability, as evidenced by increased uptake both in vitro and in vivo. Notably, lower densities of retinol are found to be more effective than higher densities. Furthermore, loading AS and JQ1 into retinol-modified chitosan NPs demonstrates the ability to reverse the activation of aHSCs, evidenced by the reduction in fibronectin, vimentin and PDGFR-β expression in GRX cells post-NP treatment making them a promising therapeutic tool for the treatment of fibrotic disorders, particularly liver fibrosis.

Author Contributions: Conceptualization, S.N.T.; funding acquisition, S.N.T. and S.M.; investigation, A.A.E. and S.K.S.-L.; methodology, A.A.E.; S.N.T. and S.K.S.-L.; resources, S.M.; S.N.T. and R.W.; supervision, S.M. and S.N.T.; visualization, A.A.E.; writing—original draft, A.A.E.; writing—review and editing, A.A.E., R.W., S.M. and S.N.T. All authors have read and agreed to the published version of the manuscript.

Funding: This research was funded by SCIENCE, TECHNOLOGY & INNOVATION FUNDING AUTHORITY (STDF), Project Number: 30133.

Institutional Review Board Statement: The animal study protocol was approved by the Ethics Committee of THE FACULTY OF PHARMACY AND BIOTECHNOLOGY AT THE GERMAN UNIVERSITY IN CAIRO (protocol code PTC-2020-09-SMH and date of approval 7 September 2020).

Informed Consent Statement: Not applicable.

Data Availability Statement: The original contributions presented in this study are included in the article Further inquiries can be directed to the corresponding authors.

Acknowledgments: We would like to express our gratitude to Mohammad Abdel-Halim from the Department of Pharmaceutical Chemistry at the Faculty of Pharmacy and Biotechnology at GUC for developing and optimizing the UPLC-MS/MS method used to quantify atorvastatin- nanoparticles encapsulation efficiency. Additionally, we would like to thank Salma Mostafa from the Department of Pharmaceutical Technology at the Faculty of Pharmacy and Biotechnology at GUC for her support during the uptake experiments.

Conflicts of Interest: The authors declare no conflicts of interest. The funders had no role in the design of the study; in the collection, analyses, or interpretation of data; in the writing of the manuscript; or in the decision to publish the results.

Abbreviations

The following abbreviations are used in this manuscript:

ANOVA	One-way analysis of variance test
AS	Atorvastatin
BDL	Bile duct ligation
BET	Bromodomain and extraterminal
BRD4	Bromodomain-containing protein 4
CDI	1,1′-carbonyldiimidazole
DMSO	Dimethyl sulfoxide
ECM	Extracellular matrix
Fl	Fluorescein
GRX	Glutaredoxin cells, murine liver connective tissue cell line
HCC	Hepatocellular carcinoma
HCV	Hepatitis C virus
HD	Hydrodynamic diameter
HRt-NPs	High Rt density
HSC	Hepatic stellate cell
IP	Intra-peritoneal
IV	Intra-venous
LRt-NPs	Low Rt density
NPs	Nanoparticles
PBS	Phosphate-buffered saline
PDGFR-β	Platelet-derived Growth Factor Receptor beta
RBP	Retinol binding protein
RES	Reticuloendothelial system
ROS	Reactive oxygen species
Rt	Retinol
SD	Standard deviation
SEM	Scanning electron microscopy
TIMPs	Tissue inhibitors of metalloproteinases
TPP	Sodium tripolyphosphate
ZP	Zeta potential
α-SMA	α-smooth muscle actin

Appendix A

Table A1. The composition of nanoparticles used in each in vitro and in vivo experiment.

Experiment	Nanoparticles Used	Section/Line
Evaluation of NPs Uptake in GRX Cells	Comparison between fluorescein-loaded unmodified nanoparticles (Fl-NPs), fluorescein-loaded nanoparticles modified with low retinol density (LRt-Fl-NPs) and fluorescein-loaded nanoparticles modified with high retinol density (HRt-Fl-NPs), in vitro.	2.4/152–192
Effect of Retinol Tagging on NP Bio-Distribution	Comparison between fluorescein-loaded unmodified nanoparticles (Fl-NPs), fluorescein-loaded nanoparticles modified with low retinol density (LRt-Fl-NPs) and fluorescein-loaded nanoparticles modified with high retinol density (HRt-Fl-NPs), in vivo.	2.5.4/245–270
Effect of Drug-Loaded NPs on Cell Viability	Comparison between JQ1-loaded unmodified nanoparticles (JQ1-NPs), JQ1-loaded nanoparticles modified with low retinol density (Rt-JQ1-NPs), atorvastatin-loaded unmodified nanoparticles (AS-NPs), atorvastatin-loaded nanoparticles modified with low retinol density (Rt-AS-NPs), in vitro.	2.6/271–283
Assessment of the Ability of Drug-Loaded NPs to Deactivate aHSCs	Comparison between JQ1-loaded unmodified nanoparticles (JQ1-NPs), JQ1-loaded nanoparticles modified with low retinol density (Rt-JQ1-NPs), atorvastatin-loaded unmodified nanoparticles (AS-NPs), atorvastatin-loaded nanoparticles modified with low retinol density (Rt-AS-NPs), or combination of both, in vitro.	2.7/284–312

Table A2. NPs size and zeta potential following surface modification with retinol.

Nanoparticle	Size (nm)	Zeta Potential (mV)
NPs	129 ± 22	41 ± 1
LRt-NPs	147 ± 10	37 ± 1
HRt-NPs	170 ± 20	29 ± 2

Table A3. Comparison of the viability (%) of different drug formulations on GRX cells using the MTT assay.

JQ1-NPs	AS-NPs	JQ1-NPs/ AS-NPs	Rt-JQ1-NPs	Rt-AS-NPs	Rt-JQ1-NPs/ Rt-AS-NPs	JQ1	AS	JQ1/AS
72%	76%	82%	69%	70%	59%	51%	74%	49%

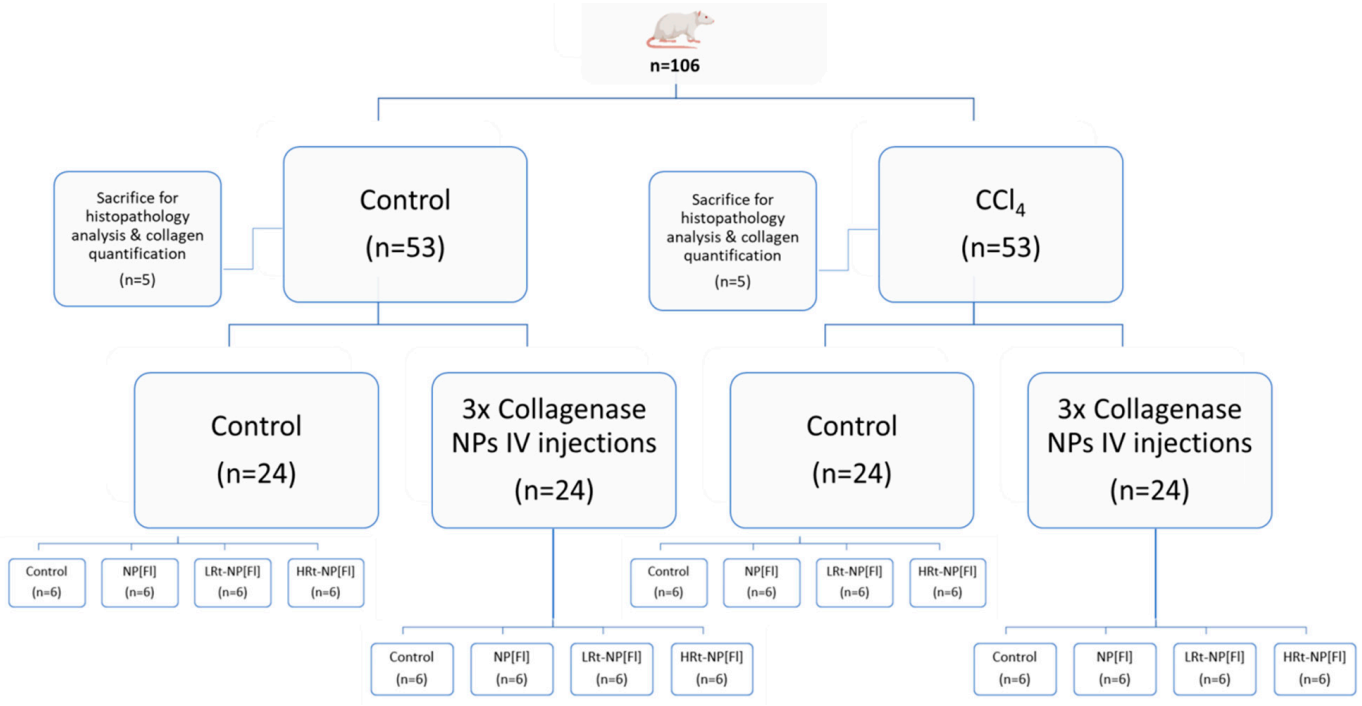


Figure A1. Schematic diagram of liver fibrosis induction and NP administration for bio-distribution analysis.

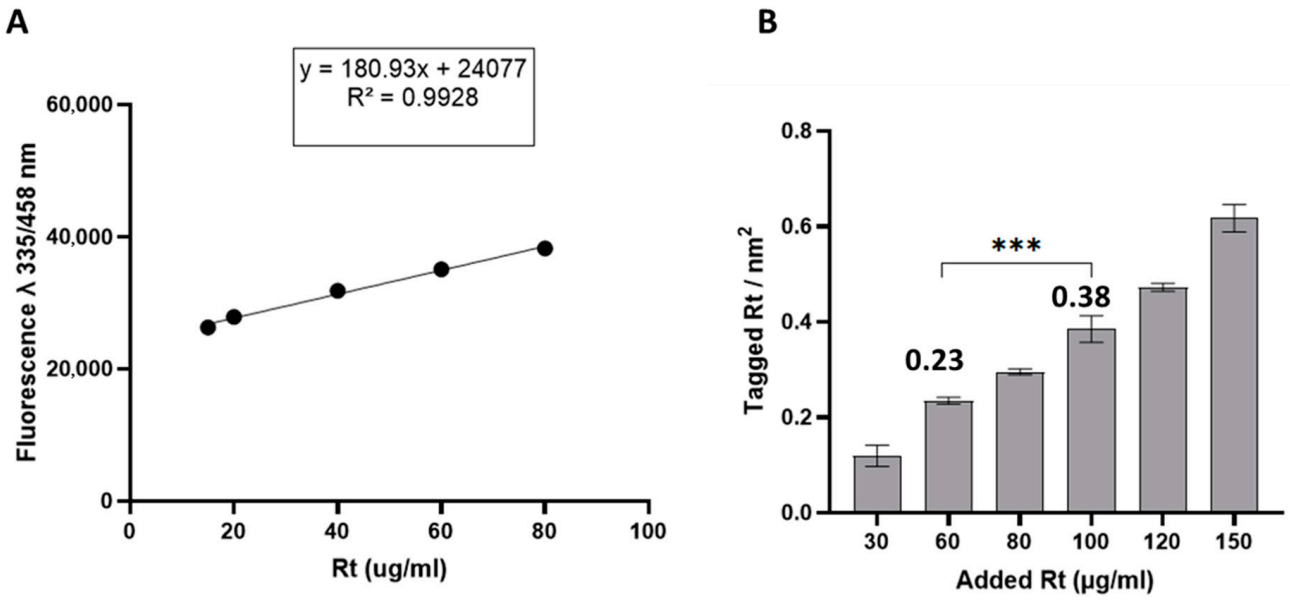


Figure A2. (**A**) Calibration curve used for retinol quantification; (**B**) no. of tagged retinol molecules per nm^2. Statistical analysis was performed using GraphPad Prism version 9.2 (GraphPad Software, San Diego, CA, USA) with one-way analysis of variance (ANOVA), where (***) $p < 0.001$.

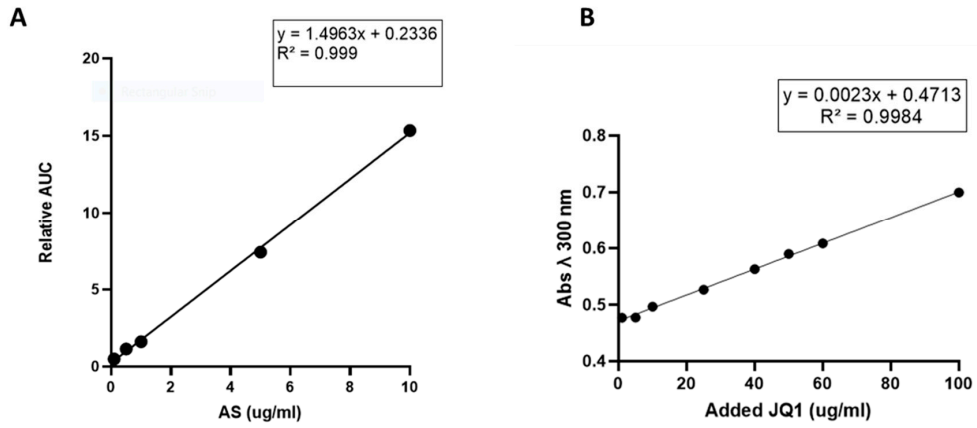


Figure A3. (**A**) Calibration curve of atorvastatin from UPLC MS/MS using diphenhydramine as the internal standard. The curve was generated based on the relative area under the curve (AUC) for samples with concentrations ranging from 0.1 to 10 µg/mL. (**B**) Calibration curve of JQ1 by spectrophotometric analysis at a wavelength of 300 nm. The curve was created using a concentration range of 1–100 µg/mL.

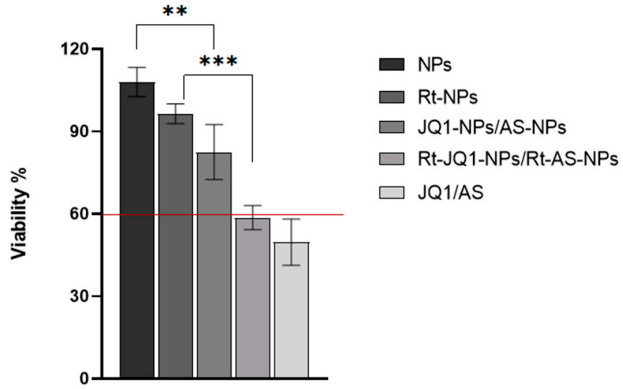


Figure A4. MTT assay of reference NPs and Rt-NPs, as well as a combination of free drugs or drug-loaded NP, and Rt-NPs at concentrations used in therapy experiment, red line marks 60% cell viability. Statistical analysis was conducted using GraphPad Prism version 9.2 (GraphPad Software, San Diego, CA, USA) with one-way analysis of variance test (ANOVA), where (**) $p \leq 0.01$ and (***) $p < 0.001$.

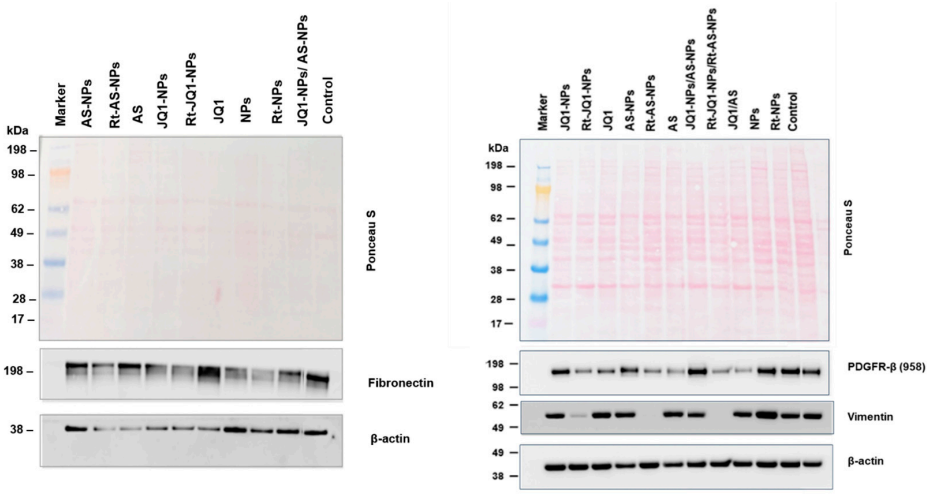


Figure A5. A representative replica of Western blot analysis depicting the expression of fibronectin, vimentin, and PDGFR-β relative to β-actin after treatment of GRX with JQ1 and AS in their free form, loaded into NPs, or retinol-modified NPs.

References

1. Antar, S.A.; Ashour, N.A.; Marawan, M.E.; Al-Karmalawy, A.A. Fibrosis: Types, Effects, Markers, Mechanisms for Disease Progression, and Its Relation with Oxidative Stress, Immunity, and Inflammation. *Int. J. Mol. Sci.* **2023**, *24*, 4004. [CrossRef]
2. Blaner, W.S.; O'Byrne, S.M.; Wongsiriroj, N.; Kluwe, J.; D'Ambrosio, D.M.; Jiang, H.; Schwabe, R.F.; Hillman, E.M.; Piantedosi, R.; Libien, J. Hepatic stellate cell lipid droplets: A specialized lipid droplet for retinoid storage. *Biochim. Biophys. Acta Mol. Cell Biol. Lipids.* **2009**, *1791*, 467–473. [CrossRef] [PubMed]
3. Friedman, S.L. Hepatic Stellate Cells: Protean, Multifunctional, and Enigmatic Cells of the Liver. *Physiol. Rev.* **2008**, *88*, 125–172. [CrossRef]
4. Wells, R.G. Cellular Sources of Extracellular Matrix in Hepatic Fibrosis. *Clin. Liver Dis.* **2008**, *12*, 759–768. [CrossRef]
5. Wells, R.G. The role of matrix stiffness in regulating cell behavior. *Hepatology* **2008**, *47*, 1394–1400. [CrossRef]
6. Arthur, M.J.P. Reversibility of liver fibrosis and cirrhosis following treatment for hepatitis C. *Gastroenterology* **2002**, *122*, 1525–1528. [CrossRef] [PubMed]
7. Simon, T.G.; King, L.Y.; Zheng, H.; Chung, R.T. Statin use is associated with a reduced risk of fibrosis progression in chronic hepatitis C. *J. Hepatol.* **2015**, *62*, 18–23. [CrossRef] [PubMed]
8. Abraldes, J.G.; Albillos, A.; Bañares, R.; Turnes, J.; González, R.; García–Pagán, J.C.; Bosch, J. Simvastatin Lowers Portal Pressure in Patients With Cirrhosis and Portal Hypertension: A Randomized Controlled Trial. *Gastroenterology* **2009**, *136*, 1651–1658. [CrossRef]
9. Nikolic, T.; Zivkovic, V.; Srejovic, I.; Stojic, I.; Jeremic, N.; Jeremic, J.; Radonjic, K.; Stankovic, S.; Obrenovic, R.; Djuric, D.; et al. Effects of atorvastatin and simvastatin on oxidative stress in diet-induced hyperhomocysteinemia in Wistar albino rats: A comparative study. *Mol. Cell. Biochem.* **2018**, *437*, 109–118. [CrossRef]
10. Ghoreshi, Z.A.S.; Kabirifar, R.; Khodarahmi, A.; Karimollah, A.; Moradi, A. The preventive effect of atorvastatin on liver fibrosis in the bile duct ligation rats via antioxidant activity and down-regulation of Rac1 and NOX1. *Iran. J. Basic Med. Sci.* **2020**, *23*, 30–35. [CrossRef]
11. Qu, M.; Zhang, X.; Hu, X.; Dong, M.; Pan, X.; Bian, J.; Zhou, Q. BRD4 inhibitor JQ1 inhibits and reverses mechanical injury-induced corneal scarring. *Cell Death Discov.* **2018**, *4*, 64. [CrossRef]
12. Stratton, M.S.; Haldar, S.M.; McKinsey, T.A. BRD4 inhibition for the treatment of pathological organ fibrosis. *F1000Research* **2017**, *6*, 1015. [CrossRef]
13. Ding, N.; Hah, N.; Yu, R.T.; Sherman, M.H.; Benner, C.; Leblanc, M.; He, M.; Liddle, C.; Downes, M.; Evans, R.M. BRD4 is a novel therapeutic target for liver fibrosis. *Proc. Natl. Acad. Sci. USA* **2015**, *112*, 15713–15718. [CrossRef]
14. Duan, Q.; McMahon, S.; Anand, P.; Shah, H.; Thomas, S.; Salunga, H.T.; Huang, Y.; Zhang, R.; Sahadevan, A.; Lemieux, M.E.; et al. BET bromodomain inhibition suppresses innate inflammatory and profibrotic transcriptional networks in heart failure. *Sci. Transl. Med.* **2017**, *9*, eaah5084. [CrossRef] [PubMed]
15. Zhou, B.; Mu, J.; Gong, Y.; Lu, C.; Zhao, Y.; He, T.; Qin, Z. Brd4 inhibition attenuates unilateral ureteral obstruction-induced fibrosis by blocking TGF-β-mediated Nox4 expression. *Redox Biol.* **2017**, *11*, 390–402. [CrossRef] [PubMed]
16. Ding, H.; Yang, X.; Tian, J.; Wang, X.; Ji, Y.; El-Ashram, S.; Ren, C.; Shen, J.; Liu, M. JQ-1 ameliorates schistosomiasis liver fibrosis by suppressing JAK2 and STAT3 activation. *Biomed. Pharmacother.* **2021**, *144*, 112281. [CrossRef]
17. Fortuna, V.A.; Martucci, R.B.; Trugo, L.C.; Borojevic, R. Hepatic stellate cells uptake of retinol associated with retinol-binding protein or with bovine serum albumin. *J. Cell. Biochem.* **2003**, *90*, 792–805. [CrossRef]
18. Senoo, H.; Kojima, N.; Sato, M. Vitamin A-Storing Cells (Stellate Cells). *Vitam. Horm.* **2007**, *75*, 131–159. [CrossRef] [PubMed]
19. Sato, Y.; Murase, K.; Kato, J.; Kobune, M.; Sato, T.; Kawano, Y.; Takimoto, R.; Takada, K.; Miyanishi, K.; Matsunaga, T.; et al. Resolution of liver cirrhosis using vitamin A–coupled liposomes to deliver siRNA against a collagen-specific chaperone. *Nat. Biotechnol.* **2008**, *26*, 431–442. [CrossRef]
20. Duong, H.T.T.; Dong, Z.; Su, L.; Boyer, C.; George, J.; Davis, T.P.; Wang, J. The Use of Nanoparticles to Deliver Nitric Oxide to Hepatic Stellate Cells for Treating Liver Fibrosis and Portal Hypertension. *Small* **2015**, *11*, 2291–2304. [CrossRef]
21. Lee, H.; Jeong, H.; Park, S.; Yoo, W.; Choi, S.; Choi, K.; Lee, M.; Lee, M.; Cha, D.; Kim, Y.; et al. Fusion protein of retinol-binding protein and albumin domain III reduces liver fibrosis. *EMBO Mol. Med.* **2015**, *7*, 819–830.
22. Pan, T.L.; Wang, P.W.; Hung, C.F.; Aljuffali, I.A.; Dai, Y.S.; Fang, J.Y. The impact of retinol loading and surface charge on the hepatic delivery of lipid nanoparticles. *Colloids Surf. B Biointerfaces* **2016**, *141*, 584–594. [CrossRef]
23. Zhang, Z.; Wang, C.; Zha, Y.; Hu, W.; Gao, Z.; Zang, Y.; Chen, J.; Zhang, J.; Dong, L. Corona-Directed Nucleic Acid Delivery into Hepatic Stellate Cells for Liver Fibrosis Therapy. *ACS Nano* **2015**, *9*, 2405–2419. [CrossRef]
24. Ezzat, A.A.; Tammam, S.N.; Hanafi, R.S.; Rashad, O.; Osama, A.; Abdelnaby, E.; Magdeldin, S.; Mansour, S. Different Serum, Different Protein Corona! the Impact of the Serum Source on Cellular Targeting of Folic Acid-Modified Chitosan-Based Nanoparticles. *Mol. Pharm.* **2022**, *19*, 1635–1646. [CrossRef]

25. Hassan, R.; Tammam, S.N.; El Safy, S.; Abdel-Halim, M.; Asimakopoulou, A.; Weiskirchen, R.; Mansour, S. Prevention of hepatic stellate cell activation using JQ1-and atorvastatin-loaded chitosan nanoparticles as a promising approach in therapy of liver fibrosis. *Eur. J. Pharm. Biopharm.* **2019**, *134*, 96–106. [CrossRef]
26. El-Safy, S.; Tammam, S.N.; Abdel-Halim, M.; Ali, M.E.; Youshia, J.; Boushehri, M.A.S.; Lamprecht, A.; Mansour, S. Collagenase loaded chitosan nanoparticles for digestion of the collagenous scar in liver fibrosis: The effect of chitosan intrinsic collagen binding on the success of targeting. *Eur. J. Pharm. Biopharm.* **2020**, *148*, 54–66. [CrossRef] [PubMed]
27. Heinemeier, K.M.; Olesen, J.L.; Haddad, F.; Langberg, H.; Kjaer, M.; Baldwin, K.M.; Schjerling, P. Expression of collagen and related growth factors in rat tendon and skeletal muscle in response to specific contraction types. *J. Physiol.* **2007**, *582*, 1303–1316. [CrossRef] [PubMed]
28. Borkham-Kamphorst, E.; Steffen, B.T.; Van de Leur, E.; Tihaa, L.; Haas, U.; Woitok, M.M.; Meurer, S.K.; Weiskirchen, R. Adenoviral CCN gene transfers induce in vitro and in vivo endoplasmic reticulum stress and unfolded protein response. *Biochim. Biophys. Acta Mol. Cell Res.* **2016**, *1863*, 2604–2612. [CrossRef]
29. Tammam, S.N.; Azzazy, H.M.E.; Lamprecht, A. Biodegradable Particulate Carrier Formulation and Tuning for Targeted Drug Delivery. *J. Biomed. Nanotechnol.* **2015**, *11*, 555–577. [CrossRef] [PubMed]
30. Noh, K.H.; Park, Y.M.; Kim, H.S.; Kang, T.H.; Song, K.-H.; Lee, Y.-H.; Byeon, Y.; Jeon, H.N.; Jung, I.D.; Shin, B.C.; et al. GM-CSF-loaded chitosan hydrogel as an immunoadjuvant enhances antigen-specific immune responses with reduced toxicity. *BMC Immunol.* **2014**, *15*, 48. [CrossRef]
31. Azzam, M.; El Safy, S.; Abdelgelil, S.A.; Weiskirchen, R.; Asimakopoulou, A.; de Lorenzi, F.; Lammers, T.; Mansour, S.; Tammam, S. Targeting Activated Hepatic Stellate Cells Using Collagen-Binding Chitosan Nanoparticles for siRNA Delivery to Fibrotic Livers. *Pharmaceutics* **2020**, *12*, 590. [CrossRef] [PubMed]
32. Cogger, V.C.; O'Reilly, J.N.; Warren, A.; Le Couteur, D.G. A Standardized Method for the Analysis of Liver Sinusoidal Endothelial Cells and Their Fenestrations by Scanning Electron Microscopy. *J. Vis. Exp.* **2015**, *98*, 52698. [CrossRef]
33. Rodde, M.S.; Divase, G.T.; Devkar, T.B.; Tekade, A.R. Solubility and Bioavailability Enhancement of Poorly Aqueous Soluble Atorvastatin: In Vitro, Ex Vivo, and In Vivo Studies. *Biomed Res. Int.* **2014**, *2014*, 463895. [CrossRef]
34. Jostes, S.; Nettersheim, D.; Fellermeyer, M.; Schneider, S.; Hafezi, F.; Honecker, F.; Schumacher, V.; Geyer, M.; Kristiansen, G.; Schorle, H. The bromodomain inhibitor JQ1 triggers growth arrest and apoptosis in testicular germ cell tumours in vitro and in vivo. *J. Cell. Mol. Med.* **2017**, *21*, 1300–1314. [CrossRef]
35. Masoudi, E.; Soleimani, M.; Zarinfard, G.; Homayoun, M.; Bakhtiari, M. The effects of chitosan-loaded JQ1 nanoparticles on OVCAR-3 cell cycle and apoptosis-related gene expression. *Res. Pharm. Sci.* **2024**, *19*, 53–63. [CrossRef]
36. Chen, Z.; Jain, A.; Liu, H.; Zhao, Z.; Cheng, K. Targeted Drug Delivery to Hepatic Stellate Cells for the Treatment of Liver Fibrosis. *J. Pharmacol. Exp. Ther.* **2019**, *370*, 695–702. [CrossRef]
37. Sun, H.; Kawaguchi, R. The Membrane Receptor for Plasma Retinol-Binding Protein, A New Type of Cell-Surface Receptor. *Int. Rev. Cell Mol. Biol.* **2011**, *288*, 1–41. [CrossRef]
38. Schröder, S.K.; Schüler, H.M.; Petersen, K.V.; Tesauro, C.; Knudsen, B.R.; Pedersen, F.S.; Krus, F.; Buhl, E.M.; Roeb, E.; Roderfeld, M.; et al. Genetic and Molecular Characterization of the Immortalized Murine Hepatic Stellate Cell Line GRX. *Cells* **2022**, *11*, 1504. [CrossRef]
39. Vicente, C.P.; Fortuna, V.A.; Margis, R.; Trugo, L.; Borojevic, R. Retinol uptake and metabolism, and cellular retinol binding protein expression in an in vitro model of hepatic stellate cells. *Mol. Cell. Biochem.* **1998**, *187*, 11–21. [CrossRef]
40. Senoo, H.; Smeland, S.; Malaba, L.; Bjerknes, T.; Stang, E.; Roos, N.; Berg, T.; Norum, K.R.; Blomhoff, R. Transfer of retinol-binding protein from HepG2 human hepatoma cells to cocultured rat stellate cells. *Proc. Natl. Acad. Sci. USA* **1993**, *90*, 3616–3620. [CrossRef]
41. Lepreux, S.; Bioulac-Sage, P.; Gabbiani, G.; Sapin, V.; Housset, C.; Rosenbaum, J.; Balabaud, C.; Desmoulière, A. Cellular retinol-binding protein-1 expression in normal and fibrotic/cirrhotic human liver: Different patterns of expression in hepatic stellate cells and (myo)fibroblast subpopulations. *J. Hepatol.* **2004**, *40*, 774–780. [CrossRef]
42. Uchio, K.; Tuchweber, B.; Manabe, N.; Gabbiani, G.; Rosenbaum, J.; Desmoulière, A. Cellular Retinol-Binding Protein-1 Expression and Modulation during In Vivo and In Vitro Myofibroblastic Differentiation of Rat Hepatic Stellate Cells and Portal Fibroblasts. *Lab. Investig.* **2002**, *82*, 619–628. [CrossRef]
43. Senoo, H.; Yoshikawa, K.; Morii, M.; Miura, M.; Imai, K.; Mezaki, Y. Hepatic stellate cell (vitamin A-storing cell) and its relative—Past, present and future. *Cell Biol. Int.* **2010**, *34*, 1247–1272. [CrossRef]
44. Luo, J.; Zhang, Z.; Zeng, Y.; Dong, Y.; Ma, L. Co-encapsulation of collagenase type I and silibinin in chondroitin sulfate coated multilayered nanoparticles for targeted treatment of liver fibrosis. *Carbohydr. Polym.* **2021**, *263*, 117964. [CrossRef] [PubMed]
45. Wu, S.; Wang, X.; Xing, W.; Li, F.; Liang, M.; Li, K.; He, Y.; Wang, J. An update on animal models of liver fibrosis. *Front. Med.* **2023**, *10*, 1160053. [CrossRef]

46. Kabir, N.; Ali, H.; Ateeq, M.; Bertino, M.F.; Shah, M.R.; Franzel, L. Silymarin coated gold nanoparticles ameliorates CCl 4 -induced hepatic injury and cirrhosis through down regulation of hepatic stellate cells and attenuation of Kupffer cells. *RSC Adv.* **2014**, *4*, 9012–9020. [CrossRef]
47. Fortea, J.I.; Fernández-Mena, C.; Puerto, M.; Ripoll, C.; Almagro, J.; Bañares, J.; Bellón, J.M.; Bañares, R.; Vaquero, J. Comparison of Two Protocols of Carbon Tetrachloride-Induced Cirrhosis in Rats—Improving Yield and Reproducibility. *Sci. Rep.* **2018**, *8*, 9163. [CrossRef] [PubMed]
48. Scholten, D.; Trebicka, J.; Liedtke, C.; Weiskirchen, R. The carbon tetrachloride model in mice. *Lab. Anim.* **2015**, *49* (Suppl. S1), 4–11. [CrossRef] [PubMed]
49. Karsdal, M.A.; Daniels, S.J.; Nielsen, S.H.; Bager, C.; Rasmussen, D.G.K.; Loomba, R.; Surabattula, R.; Villesen, I.F.; Luo, Y.; Shevell, D.; et al. Collagen biology and non-invasive biomarkers of liver fibrosis. *Liver Int.* **2020**, *40*, 736–750. [CrossRef]
50. Murphy, F.; Arthur, M.; Iredale, J. Developing strategies for liver fibrosis treatment. *Expert Opin. Investig. Drugs* **2002**, *11*, 1575–1585. [CrossRef]
51. Martinez-Hernandez, A.; Amenta, P.S. The hepatic extracellular matrix. *Virchows Arch. A Pathol. Anat. Histopathol.* **1993**, *423*, 77–84. [CrossRef]
52. Abdalla, N.M.; El Aziz, F.M.A.; Deghady, A.; Abaza, M.H.; Ellakany, W.I. Tissue inhibitor of matrix metalloprotinase-1 and collagen type IV in HCV-associated cirrhosis and grading of esophageal varices. *Egypt. Liver J.* **2024**, *14*, 11. [CrossRef]
53. Xu, Z.; Chen, Z.; Lan, T.; Han, Y.; Yang, N.; Wang, C.; Tao, M.; Li, H.; Song, Y.; Ma, X. Protective Effects of Phytic Acid on CCl4-Induced Liver Fibrosis in Mice. Arshad MS, editor. *J. Food Biochem.* **2023**, *2023*, 6634450. [CrossRef]
54. Sayed, E.A.; Badr, G.; Hassan, K.A.-H.; Waly, H.; Ozdemir, B.; Mahmoud, M.H.; Alamery, S. Induction of liver fibrosis by CCl4 mediates pathological alterations in the spleen and lymph nodes: The potential therapeutic role of propolis. *Saudi J. Biol. Sci.* **2021**, *28*, 1272–1282. [CrossRef] [PubMed]
55. Zein, N.; Yassin, F.; Ayoub, H.G.; Elewa, Y.H.A.; Mohamed, S.K.A.; Mahmoud, M.H.; Elfeky, M.; Batiha, G.E.-S.; Zahran, M.H. In vivo investigation of the anti-liver fibrosis impact of Balanites aegyptiaca/ chitosan nanoparticles. *Biomed. Pharmacother.* **2024**, *172*, 116193. [CrossRef]
56. Elzoheiry, A.; Ayad, E.; Omar, N.; Elbakry, K.; Hyder, A. Anti-liver fibrosis activity of curcumin/chitosan-coated green silver nanoparticles. *Sci. Rep.* **2022**, *12*, 18403. [CrossRef]
57. Wary, R.; Sivaraj, S.; Gurukarthikeyan, P.R.K.; Mari, S.; SURAJa, G.D.; Kannayiram, G.O.M.A.T.H.I. Chitosan gallic acid microsphere incorporated collagen matrix for chronic wounds: Biophysical and biochemical characterization. *Int. J. Pharm. Pharm. Sci.* **2014**, *6*, 94–100.
58. Wilkinson, C.M.; Kalisvaart, A.C.; Kung, T.F.; Maisey, D.R.; Klahr, A.C.; Dickson, C.T.; Colbourne, F. The collagenase model of intracerebral hemorrhage in awake, freely moving animals: The effects of isoflurane. *Brain Res.* **2020**, *1728*, 146593. [CrossRef] [PubMed]
59. Jin, B.; Alter, H.J.; Zhang, Z.-C.; Shih, J.W.-K.; Esteban, J.M.; Sun, T.; Yang, Y.-S.; Qiu, Q.; Liu, X.-L.; Yao, L.; et al. Reversibility of experimental rabbit liver cirrhosis by portal collagenase administration. *Lab. Investig.* **2005**, *85*, 992–1002. [CrossRef] [PubMed]
60. Ouchi, H.; Fujita, M.; Ikegame, S.; Ye, Q.; Inoshima, I.; Harada, E.; Kuwano, K.; Nakanishi, Y. The role of collagenases in experimental pulmonary fibrosis. *Pulm. Pharmacol. Ther.* **2008**, *21*, 401–408. [CrossRef]
61. Villegas, M.R.; Baeza, A.; Usategui, A.; Ortiz-Romero, P.L.; Pablos, J.L.; Vallet-Regí, M. Collagenase nanocapsules: An approach to fibrosis treatment. *Acta Biomater.* **2018**, *74*, 430–438. [CrossRef]
62. Dolor, A.; Szoka, F.C. Digesting a Path Forward: The Utility of Collagenase Tumor Treatment for Improved Drug Delivery. *Mol. Pharm.* **2018**, *15*, 2069–2083. [CrossRef]
63. Lin, H.; Lin, J. Treatment of oral submucous fibrosis by collagenase: Effects on oral opening and eating function. *Oral Dis.* **2007**, *13*, 407–413. [CrossRef] [PubMed]
64. Alkilany, A.M.; Zhu, L.; Weller, H.; Mews, A.; Parak, W.J.; Barz, M.; Feliu, N. Ligand density on nanoparticles: A parameter with critical impact on nanomedicine. *Adv. Drug Deliv. Rev.* **2019**, *143*, 22–36. [CrossRef]
65. Fakhari, A.; Baoum, A.; Siahaan, T.J.; Le, K.B.; Berkland, C. Controlling ligand surface density optimizes nanoparticle binding to ICAM-1. *J. Pharm. Sci.* **2011**, *100*, 1045–1056. [CrossRef]
66. Kawano, K.; Maitani, Y. Effects of Polyethylene Glycol Spacer Length and Ligand Density on Folate Receptor Targeting of Liposomal Doxorubicin In Vitro. *J. Drug Deliv.* **2011**, *2011*, 160967. [PubMed]
67. Tammam, S.N.; Azzazy, H.M.; Breitinger, H.G.; Lamprecht, A. Chitosan Nanoparticles for Nuclear Targeting: The Effect of Nanoparticle Size and Nuclear Localization Sequence Density. *Mol. Pharm.* **2015**, *12*, 4277–4289. [CrossRef]
68. Elias, D.R.; Poloukhtine, A.; Popik, V.; Tsourkas, A. Effect of ligand density, receptor density, and nanoparticle size on cell targeting. *Nanomedicine* **2013**, *9*, 194–201. [CrossRef]
69. Zanotti, G.; Berni, R. Plasma Retinol-Binding Protein: Structure and Interactions with Retinol, Retinoids, and Transthyretin. *Vitam. Horm.* **2004**, *69*, 271–295. [CrossRef]
70. Ng, C.K.F.; Chan, M.H.M.; Tai, M.H.L.; Lam, C.W.K. Hepatorenal syndrome. *Clin. Biochem. Rev.* **2007**, *28*, 11–17.

71. DiKun, K.M.; Gudas, L.J. Vitamin A and retinoid signaling in the kidneys. *Pharmacol. Ther.* **2023**, *248*, 108481. [CrossRef]
72. Calvente, C.J.; Sehgal, A.; Popov, Y.; Kim, Y.O.; Zevallos, V.; Sahin, U.; Diken, M.; Schuppan, D. Specific hepatic delivery of procollagen α1(I) small interfering RNA in lipid-like nanoparticles resolves liver fibrosis. *Hepatology* **2015**, *62*, 1285–1297. [CrossRef]
73. Cortés, H.; Alcalá-Alcalá, S.; Caballero-Florán, I.H.; Bernal-Chávez, S.A.; Ávalos-Fuentes, A.; González-Torres, M.; Carmen, M.G.-D.; Figueroa-González, G.; Reyes-Hernández, O.D.; Floran, B.; et al. A Reevaluation of Chitosan-Decorated Nanoparticles to Cross the Blood-Brain Barrier. *Membranes* **2020**, *10*, 212. [CrossRef]
74. Caprifico, A.E.; Foot, P.J.S.; Polycarpou, E.; Calabrese, G. Overcoming the Blood-Brain Barrier: Functionalised Chitosan Nanocarriers. *Pharmaceutics* **2020**, *12*, 1013. [CrossRef]
75. Wang, Z.H.; Wang, Z.Y.; Sun, C.S.; Wang, C.Y.; Jiang, T.Y.; Wang, S.L. Trimethylated chitosan-conjugated PLGA nanoparticles for the delivery of drugs to the brain. *Biomaterials* **2010**, *31*, 908–915. [CrossRef]
76. Pourtalebi Jahromi, L.; Moghaddam Panah, F.; Azadi, A.; Ashrafi, H. A mechanistic investigation on methotrexate-loaded chitosan-based hydrogel nanoparticles intended for CNS drug delivery: Trojan horse effect or not? *Int. J. Biol. Macromol.* **2019**, *125*, 785–790. [CrossRef]
77. Burlew, B.S.; Weber, K.T. Connective Tissue and the Heart. *Cardiol. Clin.* **2000**, *18*, 435–442. [CrossRef] [PubMed]
78. Qiao, J.-B.; Fan, Q.-Q.; Xing, L.; Cui, P.-F.; He, Y.-J.; Zhu, J.-C.; Wang, L.; Pang, T.; Oh, Y.-K.; Zhang, C.; et al. Vitamin A-decorated biocompatible micelles for chemogene therapy of liver fibrosis. *J. Control. Release* **2018**, *283*, 113–125. [CrossRef] [PubMed]
79. Li, F.; Yang, C.; Zhang, H.; Ma, J.; Jia, J.; Tang, X.; Zeng, J.; Chong, T.; Wang, X.; He, D.; et al. BET inhibitor JQ1 suppresses cell proliferation via inducing autophagy and activating LKB1/AMPK in bladder cancer cells. *Cancer Med.* **2019**, *8*, 4792–4805. [CrossRef] [PubMed]
80. Maggisano, V.; Celano, M.; Malivindi, R.; Barone, I.; Cosco, D.; Mio, C.; Mignogna, C.; Panza, S.; Damante, G.; Fresta, M.; et al. Nanoparticles Loaded with the BET Inhibitor JQ1 Block the Growth of Triple Negative Breast Cancer Cells In Vitro and In Vivo. *Cancers* **2019**, *12*, 91. [CrossRef]
81. Celano, M.; Gagliardi, A.; Maggisano, V.; Ambrosio, N.; Bulotta, S.; Fresta, M.; Russo, D.; Cosco, D. Co-Encapsulation of Paclitaxel and JQ1 in Zein Nanoparticles as Potential Innovative Nanomedicine. *Micromachines* **2022**, *13*, 1580. [CrossRef]
82. Sarbassova, G.; Nurlan, N.; Al shammari, B.R.; Francis, N.; Alshammari, M.; Aljofan, M. Investigating potential anti-proliferative activity of different statins against five cancer cell lines. *Saudi Pharm. J.* **2023**, *31*, 727–735. [CrossRef]
83. Haidar, M.K.; Demirbolat, G.M.; Timur, S.S.; Gürsoy, R.N.; Nemutlu, E.; Ulubayram, K.; Öner, L.; Eroğlu, H. Atorvastatin-loaded nanosprayed chitosan nanoparticles for peripheral nerve injury. Bioinspired, Biomim. *Nanobiomaterials* **2020**, *9*, 74–84. [CrossRef]
84. Wang, P.W.; Wu, T.H.; Lin, T.Y.; Chen, M.H.; Yeh, C.T.; Pan, T.L. Characterization of the Roles of Vimentin in Regulating the Proliferation and Migration of HSCs during Hepatic Fibrogenesis. *Cells* **2019**, *8*, 1184. [CrossRef]
85. Mòdol, T.; Brice, N.; de Galarreta, M.R.; Garzón, A.G.; Iraburu, M.J.; Martínez-Irujo, J.J.; López-Zabalza, M.J. Fibronectin Peptides as Potential Regulators of Hepatic Fibrosis Through Apoptosis of Hepatic Stellate Cells. *J. Cell. Physiol.* **2015**, *230*, 546–553. [CrossRef]
86. Liu, X.-Y.; Liu, R.-X.; Hou, F.; Cui, L.-J.; Li, C.-Y.; Chi, C.; Yi, E.; Wen, Y.; Yin, C.-H. Fibronectin expression is critical for liver fibrogenesis in vivo and in vitro. *Mol. Med. Rep.* **2016**, *14*, 3669–3675. [CrossRef] [PubMed]
87. Altrock, E.; Sens, C.; Wuerfel, C.; Vasel, M.; Kawelke, N.; Dooley, S.; Sottile, J.; Nakchbandi, I.A. Inhibition of fibronectin deposition improves experimental liver fibrosis. *J. Hepatol.* **2015**, *62*, 625–633. [CrossRef]
88. Attallah, A.M.; Abdallah, S.O.; Omran, M.M.; Farid, K.; Nasif, W.A.; Shiha, G.E.; Abdel-Aziz, A.-A.F.; Rasafy, N.; Shaker, Y.M. Diagnostic value of fibronectin discriminant score for predicting liver fibrosis stages in chronic hepatitis C virus patients. *Ann. Hepatol.* **2013**, *12*, 44–53. [CrossRef]
89. Greuter, T.; Shah, V.H. Hepatic sinusoids in liver injury, inflammation, and fibrosis: New pathophysiological insights. *J. Gastroenterol.* **2016**, *51*, 511–519. [CrossRef]
90. Dave, J.M.; Bayless, K.J. Vimentin as an Integral Regulator of Cell Adhesion and Endothelial Sprouting. *Microcirculation* **2014**, *21*, 333–344. [CrossRef]
91. Ivaska, J.; Pallari, H.M.; Nevo, J.; Eriksson, J.E. Novel functions of vimentin in cell adhesion, migration, and signaling. *Exp. Cell Res.* **2007**, *313*, 2050–2062. [CrossRef]
92. Tang, L.; Dai, F.; Liu, Y.; Yu, X.; Huang, C.; Wang, Y.; Yao, W. RhoA/ROCK signaling regulates smooth muscle phenotypic modulation and vascular remodeling via the JNK pathway and vimentin cytoskeleton. *Pharmacol. Res.* **2018**, *133*, 201–212. [CrossRef]
93. Wang, W.M.; Zhang, W.S.; Yang, Z.G. Vimentin (VIM) predicts advanced liver fibrosis in chronic hepatitis B patients: A random forest-derived analysis. *Eur. Rev. Med. Pharmacol. Sci.* **2022**, *26*, 5164–5177. [CrossRef]
94. Zhao, M.; Wang, L.; Wang, M.; Zhou, S.; Lu, Y.; Cui, H.; Racanelli, A.C.; Zhang, L.; Ye, T.; Ding, B.; et al. Targeting fibrosis: Mechanisms and clinical trials. *Signal Transduct. Target. Ther.* **2022**, *7*, 206. [CrossRef]

95. Ying, H.-Z.; Chen, Q.; Zhang, W.-Y.; Zhang, H.-H.; Ma, Y.; Zhang, S.-Z.; Fang, J.; Yu, C.-H. PDGF signaling pathway in hepatic fibrosis pathogenesis and therapeutics. *Mol. Med. Rep.* **2017**, *16*, 7879–7889. [CrossRef] [PubMed]
96. Klinkhammer, B.M.; Floege, J.; Boor, P. PDGF in organ fibrosis. *Mol. Asp. Med.* **2018**, *62*, 44–62. [CrossRef] [PubMed]
97. Kocabayoglu, P.; Lade, A.; Lee, Y.A.; Dragomir, A.-C.; Sun, X.; Fiel, M.I.; Thung, S.; Aloman, C.; Soriano, P.; Hoshida, Y.; et al. β-PDGF receptor expressed by hepatic stellate cells regulates fibrosis in murine liver injury, but not carcinogenesis. *J. Hepatol.* **2015**, *63*, 141–147. [CrossRef] [PubMed]
98. Lambrecht, J.; Verhulst, S.; Mannaerts, I.; Sowa, J.P.; Best, J.; Canbay, A.; Reynaert, H.; van Grunsven, L.A. A PDGFRβ-based score predicts significant liver fibrosis in patients with chronic alcohol abuse, NAFLD and viral liver disease. *EBioMedicine* **2019**, *43*, 501–512. [CrossRef]
99. Borkham-Kamphorst, E.; van Roeyen, C.R.C.; Ostendorf, T.; Floege, J.; Gressner, A.M.; Weiskirchen, R. Pro-fibrogenic potential of PDGF-D in liver fibrosis. *J. Hepatol.* **2007**, *46*, 1064–1074. [CrossRef]
100. Schaafsma, D.; McNeill, K.D.; Mutawe, M.M.; Ghavami, S.; Unruh, H.; Jacques, E.; Laviolette, M.; Chakir, J.; Halayko, A.J. Simvastatin inhibits TGFβ1-induced fibronectin in human airway fibroblasts. *Respir. Res.* **2011**, *12*, 113. [CrossRef]
101. Yildirim, M.; Kayalar, O.; Atahan, E.; Oztay, F. Anti-fibrotic effect of Atorvastatin on the lung fibroblasts and myofibroblasts. *Eur. Respir. J.* **2018**, *52*, PA991. [CrossRef]
102. Singh, R.S.; Chaudhary, D.K.; Mohan, A.; Kumar, P.; Chaturvedi, C.P.; Ecelbarger, C.M.; Godbole, M.M.; Tiwari, S. Greater efficacy of atorvastatin versus a non-statin lipid-lowering agent against renal injury: Potential role as a histone deacetylase inhibitor. *Sci. Rep.* **2016**, *6*, 38034. [CrossRef] [PubMed]
103. Fan, Z.; Jiang, H.; Wang, Z.; Qu, J. Atorvastatin partially inhibits the epithelial-mesenchymal transition in A549 cells induced by TGF-β1 by attenuating the upregulation of SphK1. *Oncol. Rep.* **2016**, *36*, 1016–1022. [CrossRef]
104. Ramos, I.; Stamatakis, K.; Oeste, C.L.; Pérez-Sala, D. Vimentin as a Multifaceted Player and Potential Therapeutic Target in Viral Infections. *Int. J. Mol. Sci.* **2020**, *21*, 4675. [CrossRef]
105. Chen, S.; Dong, S.; Li, Z.; Guo, X.; Zhang, N.; Yu, B.; Sun, Y. Atorvastatin Calcium Inhibits PDGF-ββ-Induced Proliferation and Migration of VSMCs Through the G0/G1 Cell Cycle Arrest and Suppression of Activated PDGFRβ-PI3K-Akt Signaling Cascade. *Cell. Physiol. Biochem.* **2017**, *44*, 215–228. [CrossRef] [PubMed]
106. Bravo, M.; Raurell, I.; Barberá, A.; Hide, D.; Gil, M.; Estrella, F.; Salcedo, M.T.; Augustin, S.; Genescà, J.; Martell, M. Synergic effect of atorvastatin and ambrisentan on sinusoidal and hemodynamic alterations in a rat model of NASH. *Dis. Model. Mech.* **2021**, *14*, dmm048884. [CrossRef] [PubMed]
107. Marchant, V.; Trionfetti, F.; Tejedor-Santamaria, L.; Rayego-Mateos, S.; Rotili, D.; Bontempi, G.; Domenici, A.; Menè, P.; Mai, A.; Martín-Cleary, C.; et al. BET Protein Inhibitor JQ1 Ameliorates Experimental Peritoneal Damage by Inhibition of Inflammation and Oxidative Stress. *Antioxidants* **2023**, *12*, 2055. [CrossRef] [PubMed]
108. Zhou, S.; Zhang, S.; Wang, L.; Huang, S.; Yuan, Y.; Yang, J.; Wang, H.; Li, X.; Wang, P.; Zhou, L.; et al. BET protein inhibitor JQ1 downregulates chromatin accessibility and suppresses metastasis of gastric cancer via inactivating RUNX2/NID1 signaling. *Oncogenesis* **2020**, *9*, 33. [CrossRef]
109. Wang, L.; Wu, X.; Wang, R.; Yang, C.; Li, Z.; Wang, C.; Zhang, F.; Yang, P. BRD4 inhibition suppresses cell growth, migration and invasion of salivary adenoid cystic carcinoma. *Biol. Res.* **2017**, *50*, 19. [CrossRef]
110. Tiago, M.; Capparelli, C.; Erkes, D.A.; Purwin, T.J.; Heilman, S.A.; Berger, A.C.; Davies, M.A.; Aplin, A.E. Targeting BRD/BET proteins inhibits adaptive kinome upregulation and enhances the effects of BRAF/MEK inhibitors in melanoma. *Br. J. Cancer* **2020**, *122*, 789–800. [CrossRef]
111. Xiong, C.; Masucci, M.V.; Zhou, X.; Liu, N.; Zang, X.; Tolbert, E.; Zhao, T.C.; Zhuang, S. Pharmacological targeting of BET proteins inhibits renal fibroblast activation and alleviates renal fibrosis. *Oncotarget* **2016**, *7*, 69291–69308. [CrossRef] [PubMed]
112. Wendler, C.C.; Schmoldt, A.; Flentke, G.R.; Case, L.C.; Quadro, L.; Blaner, W.S.; Lough, J.; Smith, S.M. Increased Fibronectin Deposition in Embryonic Hearts of Retinol-Binding Protein–Null Mice. *Circ. Res.* **2003**, *92*, 920–928. [CrossRef] [PubMed]
113. Strouhalova, D.; Macejova, D.; Mosna, B.; Bobal, P.; Otevrel, J.; Lastovickova, M.; Brtko, J.; Bobalova, J. Down-regulation of vimentin by triorganotin isothiocyanates—Nuclear retinoid X receptor agonists: A proteomic approach. *Toxicol. Lett.* **2020**, *318*, 22–29. [CrossRef] [PubMed]
114. Manku, G.; Wang, Y.; Merkbaoui, V.; Boisvert, A.; Ye, X.; Blonder, J.; Culty, M. Role of Retinoic Acid and Platelet-Derived Growth Factor Receptor Cross Talk in the Regulation of Neonatal Gonocyte and Embryonal Carcinoma Cell Differentiation. *Endocrinology* **2015**, *156*, 346–359. [CrossRef]

Disclaimer/Publisher's Note: The statements, opinions and data contained in all publications are solely those of the individual author(s) and contributor(s) and not of MDPI and/or the editor(s). MDPI and/or the editor(s) disclaim responsibility for any injury to people or property resulting from any ideas, methods, instructions or products referred to in the content.